IDENTIFICATION OF TLK/ASF1 AS A NOVEL PATHWAY FOR MEDIATING IL-1β-DRIVEN ACUTE MYELOID LEUKEMIA

By

Hsin-Yun Lin

A DISSERTATION

Presented to Cancer Biology Graduate Program
and the Oregon Health & Science University School of Medicine

in partial fulfillment of

the requirements for the degree of

Doctor of Philosophy

September 2022

School of Medicine
Oregon Health & Science University

CERTIFICATE OF APPROVAL

This is to certify that the PhD dissertation

of Hsin-Yun Lin

has been approved

Anupriya Agarwal, Mentor

Amanda McCullough, Co-Mentor

Philip Stork, Committee Chair

Jeffrey Tyner, Committee Member

Evan Lind, External Member

Table of Content

List of Figures

List of Tables

Abbreviations

AML – acute myeloid leukemia

ASF1A – anti-silencing function 1A histone chaperone

ASF1B – anti-silencing function 1B histone chaperone

ATM - ataxia telangiectasia mutated

ATR - ataxia telangiectasia and Rad3-related protein

CAF-1- chromatin assembly factor 1

CHAF1B – chromatin assembly factor 1 subunit B

CHK1 - checkpoint kinase 1

CMP - common myeloid progenitor

DNA-PK - DNA-dependent protein kinase

Dox - Doxycycline

E2F1 – E2F transcription factor 1

FLT3-ITD – fms related tyrosine kinase 3 internal tandem duplication

GAPDH - glyceraldehyde-3-phosphate dehydrogenase

GMP - granulocyte/monocyte progenitor

GUSB - Beta-glucuronidase

HIRA – histone cell cycle regulator

HSC – hematopoietic stem cell

IL-1β – interleukin 1β

IL-6 - interleukin 6MAPK – mitogen activated protein kinase

MDC1 - mediator of DNA damage checkpoint protein 1

MEP - megakaryocyte/erythrocyte progenitor

MLL-ENL – mixed lineage leukemia-eleven nineteen leukemia

MPP - multipotent progenitor

MYBL2 – MYB proto-oncogene like 2

NHEJ - non-homologous end joining

NPM1 – nucleophosmin 1

PCNA – proliferating cell nuclear antigen

RIF - replication timing regulatory factor 1

RPA - replication protein A

TCGA- The Cancer Genome Atlas

TLDA – TaqMan Low-Density Arrays

TLK1 – tousled-like kinase 1

TLK2 – tousled-like kinase 2

TNFα - tumor necrosis factor α

TP53 – tumor protein p53

Acknowledgements

First of all, I would like to thank my mentor Dr. Anupriya Agarwal for her guidance and support throughout my scientific journey at OHSU. Her passion for science and commitment to my professional growth has provided me invaluable learning experiences and lay a great foundation for my future scientific endeavors. I am grateful for every step of the way and will cherish all the accomplishments we have made. Next, I want to thank my co-mentor Dr. Amanda McCullough for reviewing my grant proposal and manuscript, my dissertation committee Dr. Philip Stork, Dr. Jeffrey Tyner and Dr. Evan Lind for providing feedback to this project.

I also want to acknowledge our collaborators: Dr. Travis Stracker, Dr. Marina Villamor, Dr. Shannon McWeeney, Sophia Jeng, Daniel Bottomly, and Dr. Andrew Adey for their support for this project. Additionally, thank you to the core facilities and their staff at OHSU for technical support.

As one of the senior members in the Agarwal laboratory, I am excited to see how our group has grown over the years. Not only have we helped each other on various projects, we have also learned and celebrated professional and personal achievements together. I am thankful for all the past and current Agarwal lab members I have worked with. First to Mona Hosseini, thank you for your wonderful friendship. Next, to John McClatchy, Katia Rebola, and Emily Wolfe, thanks for all your help in the lab.

To my friends at OHSU: Fatma Erylidiz, Sockchea Khou, and Frances Hsu, I enjoyed learning your culture and spending time with you. Finally, I would like to thank my parents and my sister for all of your unwavering support throughout this process across the globe. My parents encourage me to pursue my goals and my sister has always been there for me during challenging time.

Abstract

Genetic heterogeneity makes clinical interventions challenging for patients with acute myeloid leukemia (AML). Identifying and targeting common microenvironment-driven pathways should allow the development of effective therapies across AML genetic subtypes. Our laboratory has previously shown that the AML microenvironment is rich in proinflammatory cytokine interleukin-1β (IL-1β) and promotes the growth of AML progenitors. To elucidate the molecular underpinnings of IL-1β-driven AML progression, transcriptome analysis was performed and identified that *ASF1B* (anti-silencing function-1B) is one of the most differentially expressed genes in AML compared to healthy progenitors. This dissertation focuses on how *ASF1B*, and its regulator tousled-like kinase 2 (TLK2) contribute to AML cell growth and IL-1β-driven AML progression. First, we found *ASF1B* transcript and protein levels were upregulated at steady state and in response to IL-1β stimulation in major genetic subtypes of AML cells as compared to normal cells. Further, *ASF1B* activity is regulated by *TLK1* and *TLK2* kinases. Similar to *ASF1B*, protein levels for both TLKs were high in AML cells. Using an inducible shRNA system, depletion of *ASF1B*, its paralogous gene *ASF1A*, and both reduced leukemic cell growth both *in vitro* and *in vivo.* To understand how *ASF1B* contributes to IL-1β-driven AML progression, I utilized an MLL-ENL AML murine model and showed that *ASF1B* overexpression mimics IL-1β-mediated AML progression and deletion of *ASF1B* attenuated these effects. Further, I knocked down *TLK1*, *TLK2*, and both paralogous genes in AML cells and found that TLKs were also important for survival of the AML cells. Using an MLL-ENL AML model, genetic deletion of *TLK2* prolonged AML survival and delayed IL-1β-mediated AML progression. Additionally, the immunophenotyping data suggests that *ASF1B* or *TLK2* is

dispensable for normal hematopoiesis. Further, I found the TLK-ASF1 pathway impairs leukemia cell growth by slowing cell cycle progression, and modulating DNA damage pathway. Collectively, we provide strong evidence that the TLK-ASF1 pathway plays a critical role in potentiating IL-1β-dependent AML growth. Therefore, targeting the TLK-ASF1 pathway may serve as a potential therapeutic strategy to suppress microenvironmental-driven AML progression.

Chapter 1: Background and Introduction

1.1 Acute myeloid leukemia

Leukemia is a type of blood cancer caused by proliferation of abnormal white blood cells, impairing normal blood cell production in the bone marrow and immune functions (Sabattini et al., 2010). Leukemia can be classified based on 1) cell types: lymphoid cells (B cells, T cells, and NK cells) and myeloid cells (granulocytes, monocytes, erythrocytes, and platelets). 2) disease progression time: chronic and acute. Broader classifications include: acute lymphocytic leukemia (ALL), acute myelogenous leukemia (AML) (Dohner et al., 2015), chronic lymphocytic leukemia (CLL), and chronic myelogenous leukemia (CML). Leukemia occurs in both children and adults. AML is the second most common form of childhood leukemia after ALL and one of the most common adult leukemias along with CLL. AML is the deadliest type and the American Cancer Society (cancer.org) estimates there will be about 60,650 new cases of all types of leukemia and among those 20,050 new cases are AML in 2022. About 24,000 deaths result from all types of leukemia with 11,540 (almost 50%) of those deaths attributed to AML. AML is generally diagnosed in elderly people, with an average age of 68 and is slightly more common in males than in females. In addition to *de novo* AML, prior cancer treatment such as chemotherapy or ionizing radiation can also lead to therapy-related AML.

French-American-British (FAB) classification (Bennett et al., 1976) and the newer World Health Organization (WHO) classification (Arber et al., 2016) are two main systems to determine the subtypes of AML. FAB classification divides AML into M0-M7 based on morphology. Subtypes M0-M5 starts with undifferentiated cells and increases with maturity. M6 represents immature red blood cells and M7 represents immature

megakaryocytes. To better classify AML subtypes and evaluate prognosis, the WHO system divides AML into several groups based on cytogenetic abnormalities and gene mutations.

AML is a highly heterogenous and genetically complex disease (Li et al., 2016). The Cancer Genome Atlas (TGCA) sequenced 200 patients and showed almost 2,000 somatic mutations (Cancer Genome Atlas Research et al., 2013). The most common mutations include FLT3-ITD, NPM1, and DNMT3A, which also frequently occurred in other blood disorders such as myelodysplastic syndromes and myeloproliferative neoplasms that transform into AML (Papaemmanuil et al., 2016). These recurrent somatic mutations can be divided into different categories based on protein functions. One common category includes mutations in receptor tyrosine kinase-RAS pathway genes such as FLT3, KIT, and KRAS/NRAS (Groschel et al., 2015). Through the activation of signaling pathways, these mutations promote growth and survival of the hematopoietic progenitors. Another category of mutations occurs in myeloid transcription factors such as RUNX1 and CEBPA (Cancer Genome Atlas Research et al., 2013). Mutations or translocations of these transcription factors block cell differentiation and lead to accumulation of immature hematopoietic progenitors. Other categories involve DNA methylation such as DNMT3A, TET2, and IDH as well as chromatin modifiers ASXL1. Of note, mutations in epigenetic modifiers such as DNMT3A, TET2, and ASXL1 have been observed in healthy individuals with age-related clonal hematopoiesis, which is associated with increased risk of hematological disorders and AML (Jaiswal et al., 2014). Studies have shown that there is sequential acquisition of mutations during leukemogenesis. Mutations in epigenetic modifiers pre-existed in hematopoietic stem

cells (HSCs) before acquiring receptor tyrosine kinase-RAS pathway genes and NPM1 mutations (Papaemmanuil et al., 2016; Shlush et al., 2014)

Based on various genetic abnormalities, patients with AML can be divided into favorable, intermediate, and adverse risk groups, which guide physicians for ideal treatment options. European Leukemia Net (ELN) recommendations are one of the most commonly used methods. Favorable risks include *RUNX1-RUNX1T1*, *CBFB-MYH11*, mutated *NPM1* without *FLT3-ITD*, and biallelic mutated *CEBPA*. Intermediate risks include mutated *NPM1* and *FLT3-ITD*, and *MLLT3-KMT2A*. Adverse risks include mutated *GATA2-MECOM* and *DEK-NUP214*. Additionally, FLT3 gene mutations along with *TP53*, *RUNX1*, and *ASXL1* mutations tend to have worse prognosis while mutations in the *NPM1* and *CEBPA* genes are linked to better outcome (Dohner et al., 2015).

1.2 Treatment of AML and therapeutic resistance

Patients with AML have an average 5-year survival rate of 25%. Conventional chemotherapies remained the standard-of-care treatment for decades and genetic heterogeneity within, and between, patients is an ongoing challenge in treating AML (Estey and Dohner, 2006). For younger patients (usually less than 60 years of age), the treatment of AML is conducted in two phases. The first phase is induction therapy, which consists of 7 days of cytarabine plus 3 days of anthracyclines, such as daunorubicin or idarubicin, to debulk leukemia cells. If there is no residual disease, the patients receive consolidation therapy consisting of multiple rounds of high dose cytarabine accompanied by a stem cell transplant. For older patients or patients who cannot tolerate intense

chemotherapy, they are treated with low-intensity chemo with or without a targeted therapy or just a targeted therapy alone.

A number of targeted therapies have been developed and gained great success in recent years. Extensive efforts have been invested in designing targeted therapy against mutated FLT3 kinase, which is one of the most commonly mutated genes in AML, harbored by one third of patients (Antar et al., 2020). Multiple generations of FLT3 inhibitors have been developed. FLT3 mutations present in two forms: internal tandem duplications (FLT3-ITD) or a point mutation in tyrosine kinase domain (FLT3-TKD). First generation inhibitors such as sorafenib and midostaurin are less specific for FLT3 and extend their activity to other kinases, which can increase off-target toxicity and decrease efficacy in high FLT3 mutation burden. The next generations include quizartinib, crenolanib, and gilteritinib, which are more specific and potent. However, patients eventually acquire additional mutations and become resistant to the treatment within weeks to months. For example, patients developed secondary FLT3 mutations at D835 following the treatment of quizartinib or sorafenib. Furthermore, activated RAS/MAPK signaling pathway confers resistance to gilteritinib (McMahon et al., 2019). Additionally, IDH inhibitors have been developed to target mutations in IDH1 or IDH2 (ivosidenib or enasidenib) and help leukemia cells differentiate into more normal cells (McMurry et al., 2021). More recently, venetoclax, a BCL-2 inhibitor, was approved to use in combination with chemotherapy or alone to treat patients with AML (DiNardo et al., 2018; Konopleva et al., 2016). BCL-2 is an antiapoptotic protein, which neutralizes apoptotic activators and confers resistance to cell death (Letai, 2008). Although these strategies targeting cell

intrinsic changes have improved patient outcome slightly, new strategies are still needed to overcome the drug resistance in AML.

Emerging evidence suggests that in addition to intrinsic factors, extrinsic factors also play a key role during AML progression and therapeutic resistance. Healthy or leukemic hematopoietic stem and progenitor cells (HSPCs) are surrounded by the bone marrow microenvironment where they gain proliferation, survival, and differentiation signals through secreted growth factors and cytokines. The bone marrow microenvironment consists of various cell types including stromal cells and immune cells. The presence of leukemic cells also alters the surrounding bone marrow microenvironment, which in turn provides a selective advantage for the malignant clones (Carter et al., 2019). Interaction of leukemic cells and other cells types in the bone marrow microenvironment become an active area of research. To overcome intrinsic heterogeneity and therapeutic resistance, targeting common pathways regulated by the bone marrow microenvironment may provide a promising therapeutic strategy and improve outcome for patients with AML.

1.3 Inflammation as a key regulator of healthy and leukemic stem cells

The hematopoietic system carries out the important functions such as blood cell production (Orkin and Zon, 2008). At the top of the hematopoietic hierarchy, hematopoietic stem cells (HSCs) have self-renewal and differentiation capacity. HSCs can differentiate into multipotent progenitors (MPPs) and further differentiate into lineage specific progenitor cells that eventually become mature blood cells. Most adult HSCs are quiescent under steady state but can exit quiescence in response to environmental cues (Pietras et al., 2011). Inflammation is a protective immune response usually caused by

infection and injury. Proinflammatory cytokines and chemokines are produced to instruct responses of HSC to restore the homeostasis (Wilson et al., 2008).

However, chronic inflammatory state in patients with inflammatory diseases such as rheumatoid arthritis (RA) and with aging, impacts HSC fate and function. In a RA mouse model, systemic inflammation and myeloid overproduction were observed and blockade of IL-1 signaling pathway normalized the aberrant hematopoiesis (Hernandez et al., 2020). Accordingly, emerging studies have reported that there is an association of infectious or autoimmune diseases with increased risk for MDS/AML (Caiado et al., 2021; Kristinsson et al., 2011; Trowbridge and Starczynowski, 2021), as shown in **Figure 1.1.**

The cytokine network is deregulated in AML and levels of TNFα, IL-6, and IL-10 in plasma were found higher in patients with AML compared to healthy donors (Binder et al., 2018; Sanchez-Correa et al., 2013). A study has shown that TNFα enhanced the survival of leukemic cells through the activation of the JNK-AP1 pathway in parallel to NF-κB and blockade of the TNF-JNK-AP1 pathway sensitized cells to the NF-κB inhibitor (Volk et al., 2014). Another study reported that a subset of leukemic cells expressing both TNFα and IL-1β and dual inhibition of TNFα and IL-1β synergized with the NF-κB inhibitor, eliminating leukemic cells both *ex vivo* and *in vivo* (Li et al., 2017). Elevated levels of IL-6 interfered with red blood cell differentiation and its blockade improved anemia and prolonged survival using a mouse model of AML (Zhang et al., 2020). Using *ex vivo* cell viability screen, cytokines such as IL-1α, IL-1β, GM-CSF, IL-3, and TNFα were found to promote AML cell growth (Carey et al., 2017). Several studies have shown aberrant IL-1 signaling in preleukemic and leukemic cells, which will be discussed in the following section.

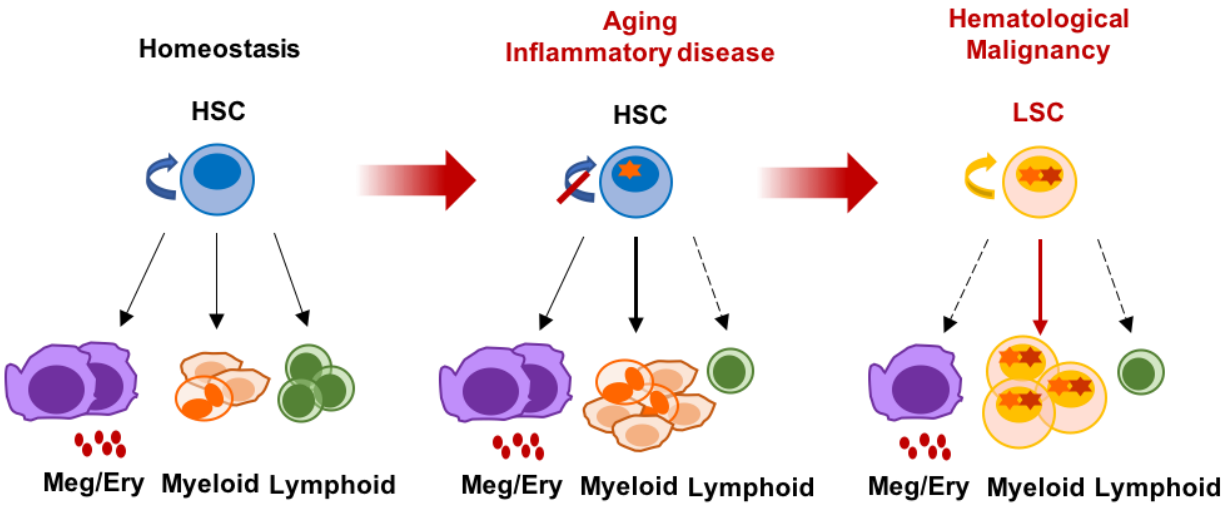

Figure 1.1. Role of inflammation in hematopoietic stem cell (HSC) and leukemic stem cell (LSC). Chronic inflammation skews lineage output and impairs self-renewal capacity of HSC. Chronic inflammation may drive the transformation of HSC to LSC. Adapted from Blood (Pietras, 2017).

1.4 Interlelukin-1 pathway and its role in acute myeloid leukemia

Interleukin 1 (IL-1) was the first interleukin discovered in the IL-1 family and has two different forms: IL-1α and IL-1β, which signal through IL-1 receptor type 1 (IL-1R1) (**Figure 1.2)**. Regulation of IL-1α and IL-1β is different but their biological activities are similar (Sims and Smith, 2010). IL-1α functions as a membrane-bound cytokine while IL-1β only actives as a secreted form. Prior to the secretion of active IL-1β, pro-IL-1β is converted by caspase-1. Upon binding of IL-1β, IL-1R1 forms dimerization with IL-1 receptor accessory protein (IL-1RAcP), which recruit myeloid differentiation primary response gene 88 (MyD88) and activate Interleukin-1 receptor-associated kinase 4 (IRAK4). Phosphorylation of IRAK4 subsequently phosphorylates IRAK1 and IRAK2, which is followed by the recruitment and oligomerization of TNFα receptor associated factor 6 (TRAF6). TRAF6 further activates transcription factor such as nuclear factor kappa B (NFκB), c-Jun N-terminal kinase (JNK), and p38 MAPK pathways. NFκB induces transcription of IL-1 responsive genes such as IL-6, IL-8, MCP1, and COX2, as shown in **Figure 1.2**. IL-1β serves as a key emergency signal and is activated in response to infection and injury to produce myeloid cells. IL-1β also stimulates the release of other cytokines and plays a crucial role in innate and adaptive immune responses.

IL-1β modulated HSC functions. A study showed that acute administration of IL-1β accelerated myeloid differentiation of HSCs and myeloid regeneration after bone marrow injury *in vivo*. However, chronic IL-1β exposure impaired self-renewal capacity of HSCs and this effect was reversible upon IL-1β withdrawal (Pietras et al., 2016).

Prior studies from our laboratory and others identified that the bone marrow microenvironment in AML is inflammation-rich and exerts inflammatory stress on healthy

and leukemic HSPCs. Through an ex vivo screening of 94 cytokines, our lab identified that IL-1β has the most profound effect on AML cell growth while suppressing the growth of normal progenitors. Higher levels of IL-1β and IL-1R1 were observed in patients with AML and patients are dependent on IL-1 signaling irrespective of their genetic subtypes. Treatment with p38MAPK inhibitor successfully suppressed IL-1β-mediated AML growth and recovered normal progenitors (Carey et al., 2017). Moreover, IL-1β downstream effectors are overexpressed or hyperactivated in primary AML cells. IL-1RAcP was found overexpressed in HSPCs of primary AML cells. Depletion of IL-1RAcP in AML cell lines decreased clonogenicity and increased apoptosis (Barreyro et al., 2012). Our previous study showed that genetic knockdown of IRAK1 in AML cells reduced their viability and leukemia burden in a mouse xenograft model. This study used pacritinib, a multi-kinase inhibitor that targets FLT3, JAK2, and IRAK1. Pacritinib reduced phosphorylation of IRAK1 in AML cells across different genetic subtypes which is not limited to FLT3 and JAK2 (Hosseini et al., 2018). Further, MLL fusion proteins are responsible for causing leukemia. A study showed that IL-1 pathway regulated the stability of wild-type MLL proteins, which displaced MLL fusion proteins in AML cells. Using a murine model of AML, pharmacologically inhibiting IRAK1/4 delayed AML progression and prolonged survival (Liang et al., 2017). Additionally, another study found a subset of AML cells primarily expressed an IRAK4 long form IRAK4-L result in maximal activation of downstream signaling and associated with poorer prognosis. This study also revealed a genetic link to U2AF1, a common splice mutation AML, which mediated expression of IRAK4-L (Smith et al., 2019). In addition to AML, IL-1 signaling is also deregulated in other hematological disorders such as MDS. TRAF6 was found overexpressed in HSPCs which accounted

for impaired hematopoiesis. This study identified hnRNPA1, a ubiquitination substrate of TRAF6, altered RNA splicing and caused HSC defects in MDS (Fang et al., 2017). IL-1 regulated AML cells in both autocrine and paracrine manners. IL-1β was secreted by AML progenitors, monocytes, and stromal cells (Carey et al., 2017; De Boer et al., 2021). IL-1β activated COX-2/PGE2 axis in stromal cells, which in turn altered β-Catenin/ARC signaling in AML cells and augmented their chemoresistance (Carter et al., 2019). Together, these studies demonstrated that IL-1 signaling is activated in AML cells and may be an important axis for therapeutic targeting in patients with AML.

Currently, there are several FDA-approved IL-1 blocking reagents (Arranz et al., 2017). Anakinra is the recombinant form of the naturally existing IL-1 receptor antagonist (IL-1RA), which reduces the activity of both IL-1α and IL-1β and has been approved for treatment of rheumatoid arthritis and other diseases (Dinarello et al., 2012). Another IL-1 blockade is canakinumab, a monoclonal antibody that specifically binds and neutralizes human IL-1β result in blocking the interaction with IL-1R1. Canakinumab is being evaluated in multiple clinical trials including in patients with rheumatoid arthritis (Gram, 2016). While it does not block IL-1α signaling, canakinumab has a longer half-life compared to anakinra, which is an advantage given longer and lasting effects of inflammation.

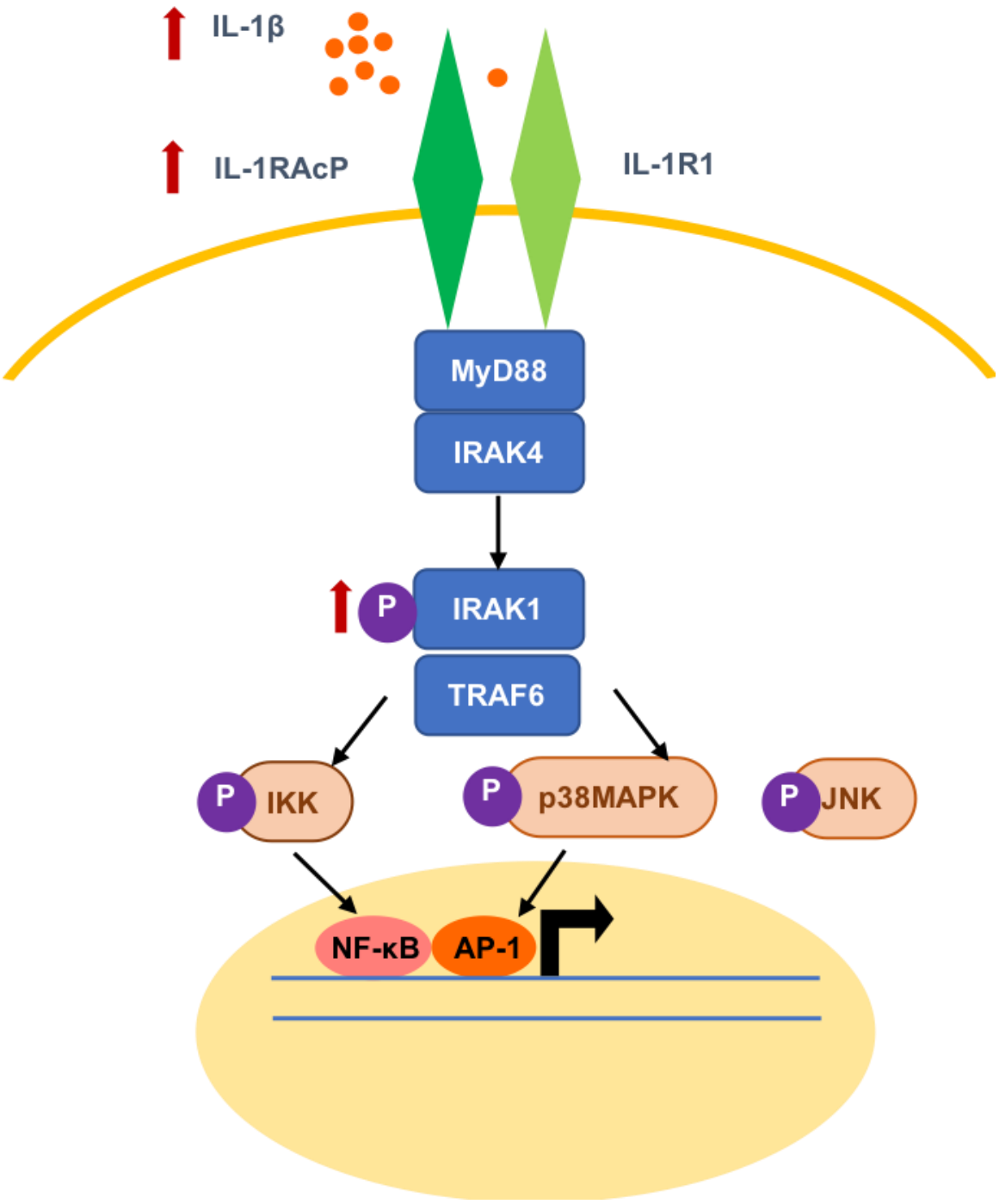

Figure 1.2. IL-1 signaling is dysregulated in AML cells. Secreted IL-1β binds to IL-1R1 and triggers a signaling cascade involving MyD88, IRAK1/4, TRAF6, p38MAPK, and NF-κB activation (Binder et al., 2018).

1.5 TLK-ASF1 pathway

1.5.1 Structure and function of ASF1

ASF1 is a histone chaperone, which escorts histones to form nucleosome cores that consist of histone H2A, H2B, H3 and H4 wrapped by 147 bp of DNA (Kornberg, 1974) during DNA replication and DNA damage repair (Groth et al., 2007; Park and Luger, 2008). ASF1 consists of an N-terminal 155-residue immunoglobulin-like domain (ASF1-NT) and an unstructured C-terminal tail, which is highly enriched in acidic residues. N-terminal of ASF1 binds to histone H3-H4 dimers in a manner preventing heterotetramer formation (English et al., 2006).

Histone chaperones are classified based on their selectivity for H2A-H2B or H3-H4. H3 variants have been discovered and may exert different functions. Replicative H3 variants are H3.1 and H3.2 while non-replicative H3 variant H3.3 is cell-cycle independent (Martire and Banaszynski, 2020). H3.3 can be substituted for canonical histones H3.1 and H3.2 when their deposition is impaired. The deposition of H3.1 and H3.2 is mediated by chromatin assembly complex 1 (CAF-1) during DNA replication. The deposition of H3.3 is independent of DNA replication and is medicated by histone regulator A (HIRA) and death domain associated protein 6 (DAXX) in association with the chromatin remodeler alpha thalassemia/mental retardation, X-linked syndrome (ATRX). ASF1 is a H3-H4 histone chaperone that delivers histones to both CAF-1 and HIRA. Additionally, ASF1 cooperates with the replicative helicase MCM2-7 to regulate histone recycling onto newly synthesized DNA.

ASF1 includes two paralogus genes, *ASF1A* and *ASF1B*, which are conserved from yeast to human cells (Abascal et al., 2013). *ASF1A* and *ASF1B* share the same histone

chaperone domain and are distinguishable by their C-terminal tails (**Figure 1.3**). *ASF1A* and *ASF1B* also exert different functions. For example, *ASF1A* but not *ASF1B*, cooperates with acetyltransferase CBP/p300 to acetylate histone H3 at lysine 56 (H3K56Ac), which is an important histone mark for chromatin disassembly and active transcription (Battu et al., 2011; Das et al., 2009). It has been shown that in breast cancer cells, ASF1B expression peaks at the S phase while ASF1A is expressed in both quiescence cells and throughout the cell cycle (Corpet et al., 2011). Both ASF1A and ASF1B are substrates of Tousled-like kinases (TLKs) and can be phosphorylated at their C-terminus. TLKs phosphorylate ASF1A during DNA replication on its C-terminal tail residues S166, S175, S192 and S199. TLKs phosphorylate ASF1B on residues S169 and S198 (Klimovskaia et al., 2014). ASF1A can also be phosphorylated by DNA-dependent protein kinase (DNA-PK) at S192 (Huang et al., 2020) and by CHK1 at S166 (Lee and Dutta, 2021).

ASF1s play important roles in double-strand break (DSB) repair. In mammalian cells, there are two major DSB repair pathways, non-homologous end-joining (NHEJ) and homologous recombination (HR) based on the phases of the cell cycle and the nature of the DNA end restriction. NHEJ participates in all phases of the cell cycle while HR mainly occurs in S/G2 phases (Delacote and Lopez, 2008). DSB repair pathway choice is also controlled by the NHEJ-promoting protein, 53BP1, and HR-promoting protein, BRCA1 (Panier and Boulton, 2014). Recent studies showed that ASF1A plays a role in both NHEJ and HR mediated pathways independent of its histone chaperone activity (Abascal et al., 2013; Corpet et al., 2011; Lee and Dutta, 2021; Lee et al., 2017; O'Sullivan et al., 2014). CHK1-mediated phosphorylation of ASF1A at S166 facilitates its interaction with mediator

of DNA damage checkpoint protein 1 (MDC1) at DSBs and the subsequent signaling cascade. Briefly, phosphorylation of ASF1A promoted ataxia telangiectasia mutated (ATM) phosphorylation of MDC1, which triggered the ubiquitination of phosphorylation of H2AX and recruitment of 53BP1 at DSBs in G1 phase (Lee and Dutta, 2021). Moreover, both ASF1A and ASF1B were recently implicated in promoting non-homologous end joining (NHEJ) through interactions with replication timing regulatory factor 1 (RIF1) (Feng et al., 2022; Tang et al., 2022). ASF1 forms a histone chaperone complex with RIF1, which suppress the resection of DSBs by breast cancer gene 1 (BRCA1)-dependent DNA end restriction, a prerequisite for homology directed repair (HDR). In additional to NHEJ, ASF1 also play crucial roles in HDR. One key DDR signaling pathway is the ataxia telangiectasia and Rad3-related protein (ATR)- checkpoint kinase 1 (CHK1) pathway. ATR is activated by replication protein A (RPA) that binds to single-stranded DNA (ssDNA) and subsequently phosphorylates CHK1, causing cell cycle arrest and initiation of a signaling cascade that includes Rad51. Huang et al found that ASF1 was phosphorylated by DNA-PK at S192, which promoted the recruitment of Rad51 loader TONSL-MMS22L to DSBs and facilitated Rad51 assembly onto ssDNA during HR (Huang et al., 2020). Additionally, ASF1A is crucial for post-repair H3K56Ac restoration, which in turn is needed for the dephosphorylation of γ-H2AX and cellular recovery from check point arrest (Battu et al., 2011). In summary, ASF1 plays multiple functions in DSB repair in a histone chaperone dependent or independent manners and its role in DSB repair remains to be determined in different cancer cell types.

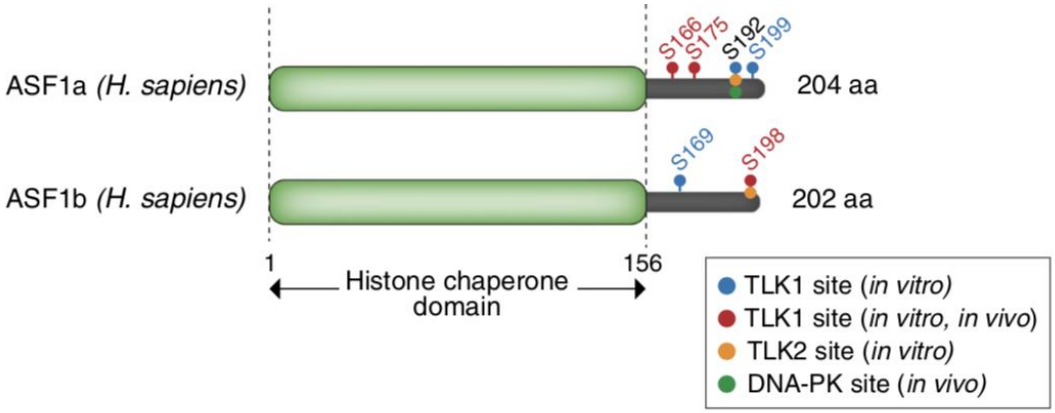

Figure 1.3. Structure of ASF1. Human ASF1A and ASF1B include a histone chaperone domain and a C-terminal tail, where the phospho-sites are identified. Adapted and used with permission from Cellular and Molecular Life Science (Segura-Bayona and Stracker, 2019).

1.5.2 Structure and function of Tousled-like kinases (TLKs)

TLKs are nuclear serine and threonine kinases and homologues of a Tousled (TSL) gene. TSL was first identified in plant *Arabidopsis thaliana* and its mutant caused a delay in flower development (Roe et al., 1993). TLKs have two paralogs, TLK1 and TLK2, which are 84% identical at the protein level (Sillje et al., 1999). The structures of TLKs include a large N-terminal regulatory domain and a C-terminal protein kinase catalytic domain (**Figure 1.4**). Coiled coil domains at the regulatory domain are required for oligomerization and activation of TLK kinase activity (Segura-Bayona and Stracker, 2019). Biochemical studies demonstrated that TLK2 is activated through autophosphorylation and cannot be activated without dimerization and oligomerization. In addition to dimerizing with itself, TLK2 can also heterodimerize with TLK1 at the first coiled coil domain. TLK1 and TLK2 have 96% identity in the kinase domain. A recent study shows that the TLK2 N-terminal region acts as a docking site for the kinase domain to facilitate phosphorylation of the C-terminal tail of ASF1 (Simon et al., 2022).

Phosphorylation of ASF1 by TLK1 or TLK2 increases its binding affinity for the histone H3-H4 dimer and promotes interactions with downstream histone chaperones CAF1 and HIRA (Klimovskaia et al., 2014; Pilyugin et al., 2009). Depletion of TLK impaired *de novo* deposition of both H3.1 and H3.3 (Lee et al., 2018). In addition to ASF1s, TLK1 has been shown to phosphorylate other substrates such as RAD9, part of the PCNA-like clamp loader complex RAD9-RAD1-HUS1 (9-1-1) during the DNA damage response (Awate and De Benedetti, 2016; Kelly and Davey, 2013).

TLK2 protein levels are regulated by cryptochrome circadian regulator 2 (CRY2) (Correia et al., 2019), an E3-ubiquitin ligase and MYBL2 was previously identified as a proximal

interactor of TLK2, although the functional relevance of this interaction remains unclear (Pavinato et al., 2022).

Several studies have shown TLKs play important roles in cell cycle progression and DNA damage responses. In response to ionizing radiation induced DSBs, CHK1 is activated by ATM and inhibited TLK1 activity via phosphorylation of its C-terminal S695 residue to prevent cell cycle progression (Groth et al., 2003). Concomitantly, phosphorylation of RAD9 at T355 mediated by TLK1 was also reduced (Kelly and Davey, 2013). It has been shown that in response to DNA damage, TLK2/ASF1A axis was required for G2/M recovery via regulation of the pro-mitotic genes (Bruinsma et al., 2016).

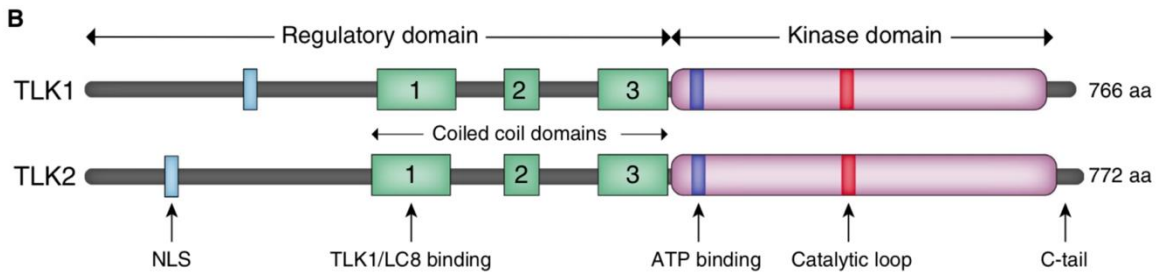

Figure 1.4. Structure of TLK. Human TLK1 and TLK2 have a regulatory domain and a kinase domain. The regulatory domain includes a nuclear localization signal and coiled coil domains, which are important for dimerization and oligomerization. The kinase domain includes ATP binding sites, a catalytic loop, and a C-terminal tail. Adapted and used with permission from Cellular and Molecular Life Science (Segura-Bayona and Stracker, 2019).

1.6 Role of the TLK-ASF1 pathway in cancer

Notably, elevated expression of both ASF1 and TLK has been described in a variety of cancers and is associated with poor prognosis (Corpet et al., 2011; Kim et al., 2016; Lee et al., 2018). How ASF1 or TLK protein abundance contributes to different cancer types is not fully understood. A recent study reported that a deubiquitinase USP52 removed ubiquitins from poly-ubiquitinated ASF1A and increased its protein stability and level. Both USP52 and ASF1A are overexpressed in breast cancer and knockdown of USP52 destabilized ASF1A, impairing cell cycle progression and chromatin assembly. Disruption of USP52-ASF1A axis also sensitizes breast cancer cells to genotoxic reagents, suggesting that ASF1A may confer higher DNA damage tolerance (Yang et al., 2018). Using an *in vivo* CRISPR screen, a study has shown that loss of ASF1A sensitized tumors to anti-PD-1 immunotherapy in a *Kras*^{G12D}/*Trp53*$^{-/-}$ lung adenocarcinoma mouse model. Their data revealed that Asf1A deficiency upregulated GM-CSF expression and promoted immunogenic macrophage differentiation and T-cell activation (Li et al., 2020). This study demonstrated that ASF1A inhibition may modulate the immune microenvironment and augment immunotherapy. In liver and prostate cancer cells, ASF1A knockdown increased p53 and p21cip1 levels, growth arrest, and DNA damage thereby triggering a cellular senescence pathway (Wu et al., 2019). In breast cancer cells, ASF1B expression peaks at the S phase while ASF1A was expressed in both quiescence cells and throughout the cell cycle. ASF1B depletion, but not ASF1A depletion, significantly reduced proliferation and ASF1B overexpression correlated with disease outcome. This study suggested that breast cancer cells may depend more on ASF1B, which may also serve as a biomarker for breast cancer prognosis (Corpet et al., 2011). SET domain containing 2 (SETD2) is a

histone H3 lysine 36 trimethyltransferase (H3K36me3) that is mutated in clear cell renal cell carcinoma. A study found that loss of SETD2-mediated H3K36me3 increased chromatin association of ASF1 and H3K56ac levels, promoting accessibility of chromatin and transcription. ASF1 inhibition increased apoptosis in SETD2-muted cells, suggesting a therapeutic vulnerability in this subtype of kidney cancer (Xie et al., 2022).

Amplification of TLK2 was found in ~ 10% of luminal estrogen receptor-positive (ER+) breast cancer and overexpression of TLK2 correlated with worse outcome despite endocrine therapy. TLK2 overexpression in breast cancer cell lines promoted metastasis through the activation of the EGFR/SRC/FAK signaling and increased cell invasion and migration. Additionally, TLK2 inhibition alone or in combination with tamoxifen, a common endocrine therapy in a xenograft model prolonged survival *in vivo* (Kim et al., 2016). Multivariate analysis using the TCGA database shows that elevated TLK1 or TLK2 expression correlated with poor prognosis in several cancer types including uveal melanoma and cervical cancer (Lee et al., 2018). Depletion of TLK2, but not TLK1, in a breast cancer cell line reduced replication-coupled chromatin assembly, increased DNA damage, and sensitized cells to checkpoint inhibitors PARP1 and CHK1 (Lee et al., 2018). Mechanistically, activation of TLK2 may reduce replication stress in proliferating cancer cells and targeting TLK2 with checkpoint inhibitors promoted synthetic lethality in cancer cells.

1.7 Targeting the TLK-ASF1 pathway in cancer

Recently, a new peptide inhibitor was developed to interfere with the binding of ASF1 to histones (Bakail et al., 2019). The peptide inhibitor is designed based on residues on H3 and H4, which can bind to ASF1 directly. ASF1 inhibition impaired cell proliferation, cell

cycle progression, and cell migration *in vitro*. Application of this inhibitor also reduced tumor size *in vivo*. This study suggested that the ASF1 peptide inhibitor has great therapeutic potential and should be further tested in other cancer models.

Kim et al screened two PKC inhibitors Go6983 and GF109203X that exhibited relative specificity for TLK2 kinase activity. Both Go6983 and GF109203X inhibited kinase activity and reduced breast cancer cell viability at a high concentration (Kim et al., 2016). The crystal structure of the TLK2 kinase domain has been described and several inhibitors, such as Cdk-1 inhibitor and GSK3-inhibitor, showed effective TLK2 inhibition. This study further analyzed the docking of these inhibitors with TLK2 which can provide valuable information for designing more potent and specific TLK2 inhibitors (Mortuza et al., 2018).

An anti-psychotics compound belonging to the phenothiazine family, thioridazine (THD) was identified (Ronald et al., 2013). The THD inhibitor reduced TLK1 activity and blocked TLK-mediated phosphorylation of Rad9 at S328, which resulted in impaired DSB repair and recovery. Recently, a phenothiazine analog, J54, was synthesized and evaluated in prostate cancer (Singh et al., 2020). After androgen deprivation therapy, increased expression of TLK1B was observed in prostate cancer cells and activation of the NEK1-ATR axis which is a key pathway for DDR (Singh et al., 2019a; Singh et al., 2019b). J54 also increased efficacy of ADT in inducing apoptosis both *in vitro* and *in vivo* suggesting a promising therapeutic angle of TLK1 in prostate cancer.

1.8 Hypothesis/Thesis Aims

Previously, we have shown that IL-1β promotes AML progression while suppressing normal hematopoiesis. In order to understand how IL-1β drives AML progression, we applied transcriptomic analysis and revealed that ASF1B (Anti-Silencing Function 1B) is one of the most up-regulated genes in AML progenitors upon IL-1β stimulation. ASF1B is regulated by TLK 1 and TLK2 kinases. Therefore, I hypothesize that IL-1β promotes AML progression through upregulation of the TLK-ASF1 pathway. The first aim is to understand how IL-1β regulates the TLK-ASF1 pathway, identify the role of ASF1 in AML, and define how ASF1 contributes to AML progression. The second aim is to identify the role of TLKs in AML and understand how these TLKs contribute to AML progression.

Chapter 2: Role of ASF1 in AML progression

2.1 Results

2.1.1 Gene expression profiling identifies ASF1B upregulation in AML progenitors upon IL-1β stimulation.

We previously found that aberrant IL-1β signaling promotes the growth of AML progenitors and suppresses healthy progenitors simultaneously (Carey et al., 2017). To reveal the cell-intrinsic differences between AML and healthy progenitors downstream of IL-1β signaling, our laboratory has performed RNA-sequencing (RNA-seq) analysis of AML and healthy bone marrow $CD34^+$ progenitors treated with and without IL-1β from three independent patient samples **(Fig.2.1A, B)**. This study identified 66 differentially expressed genes in AML progenitors and healthy progenitors upon IL-1β exposure (FDR < 0.05, $P_{adj} < 0.05$).

Gene ontology analysis using STRINGdb (string-db.org) revealed that upregulated genes in AML progenitors upon IL-1β stimulation belong to biological processes including response to cytokines (*ICAM1, BIRC3, CD40*) as well as cell cycle and chromatin organization (*ASF1B, MAD2L1, CCNA2, HIST1H1B, and HIST1H2AJ*) (**Fig. 2.1C**) (Szklarczyk et al., 2021). To further validate our findings from RNA-Seq analysis, we analyzed an additional set of AML patient samples harboring diverse genetic mutations such as FLT3-ITD and NPM1, using the TaqMan Low Density Array (TLDA), a quantitative PCR analysis, to assess expression of top differentially expressed genes, along with additional genes associated with the IL-1β signaling and related pathways (Table 1). Consistent with our RNA-seq data, TLDA revealed that *ASF1B* has larger fold

changes in AML versus healthy progenitors (**Fig. 2.1D**). Higher ASF1 expression was associated with poor prognosis in solid tumors, such as breast and cervical cancer (Corpet et al., 2011; Liu et al., 2020; Ma et al., 2021). However, to the best of our knowledge, its role has not been described previously in hematopoiesis and leukemia. Therefore, we focused on understanding the role of ASF1B in AML progression at steady state and under inflammatory stress.

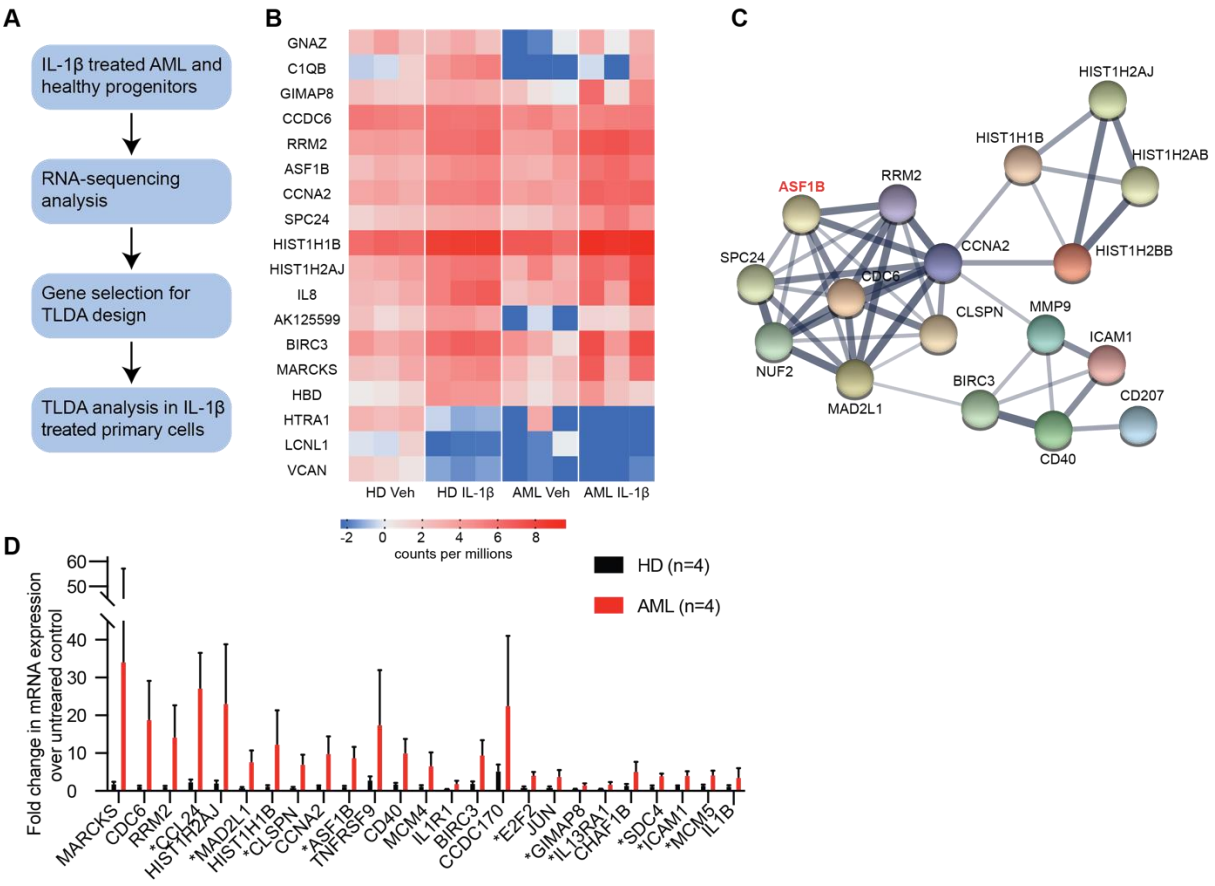

Figure 2.1. Transcriptomic analysis identifies ASF1B upregulation in AML progenitors upon IL-1β stimulation. (A) Overview of experimental design to evaluate differentially expressed genes in AML versus healthy progenitors with and without IL-1β stimulation. (B) RNA-sequencing analysis was performed on purified CD34$^+$ cells derived from the bone marrow of patients with AML (n = 3) and healthy individuals (n = 3). Cells were cultured with 10 ng/ml IL-1β or vehicle control for 2 days. The heatmap indicates the fold difference of gene expression in IL-1β-treated over untreated control in AML and healthy CD34+ bone marrow cells. Scale bar indicates counts per million. (C) Network analysis of genes upregulated by IL-1β in AML cells using STING database. (D) TaqMan low density array (TLDA) analysis was performed on AML (n = 4) and healthy CD34$^+$ bone marrow cells (n = 4) treated with or without 10 ng/ml IL-1β for 2 days. The expression of the listed genes is shown as a fold difference upon IL-1β stimulation compared to respective vehicle controls in AML and healthy CD34+ bone marrow cells.

2.1.2 Expression of ASF1 and TLK is upregulated in AML across genetic subtypes

ASF1B, and its paralogous gene ASF1A, are regulated by TLK1 and TLK2 kinases (**Fig. 2.2A**), which are amplified in several types of solid tumors (Kim et al., 2016; Lee et al., 2018). Therefore, we first determined the baseline levels of TLK and ASF1 isoforms in healthy mononuclear or $CD34^+$ progenitor cells, as compared to AML cells derived from patients with common genetic subtypes including FLT3-ITD, NPM1, MLL-ENL (**Fig. 2.2B**). We found that *TLK2* and *ASF1B* expression were upregulated 1.5- and 2.6-fold, respectively, in AML compared to healthy progenitors. On the other hand, the expression of *TLK1* and *ASF1A* was only 1- and 1.3-fold higher in AML versus healthy progenitors (**Fig. 2.2B**). *TLK1, TLK2, ASF1A,* and *ASF1B* were highly expressed and comparable across various AML cell lines (**Fig. 2.3A**). The Cancer Cell Line Encyclopedia (CCLE) database also shows higher expression of *ASF1B* across cancer types (**Fig. 2.3B**) (Barretina et al., 2012). Accordingly, the DepMap CRISPR data show most of these AML cell lines are highly dependent on ASF1B, ASF1A, and TLK2, and less dependent on TLK1 (**Fig. 2.3C**) (http://depmap.org/portal/). Further, similar to IL-1 and IL1RAP studies, we did not find any significant correlation of *ASF1B* expression levels with any particular genetic subtype of AML using Beat AML (Tyner et al., 2018) and TCGA data sets (data not shown) (Gao et al., 2013), suggesting a broader role of TLKs and ASF1B across various genetic AML subtypes.

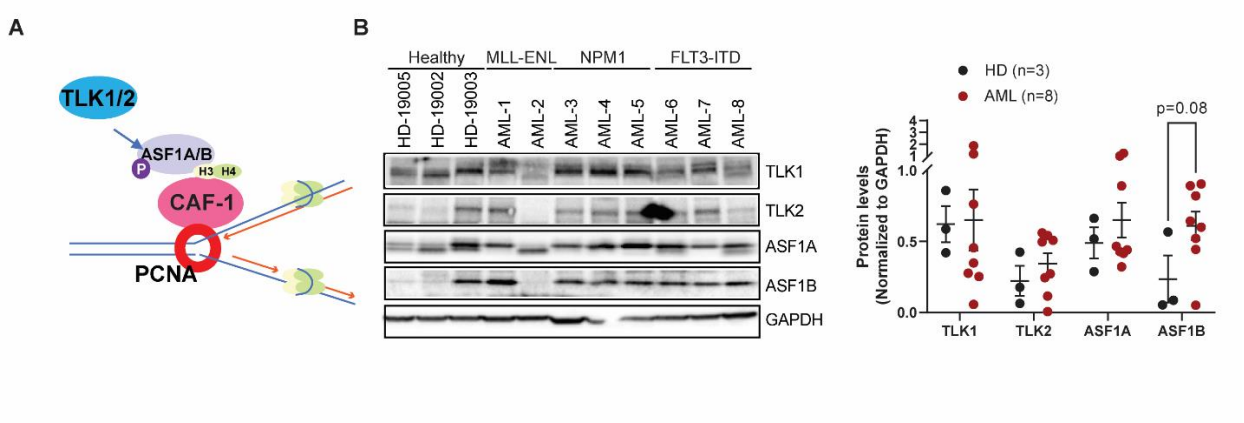

Figure 2.2. Expression of ASF1 and TLK is upregulated in AML across genetic subtypes and upon IL-1β stimulation. (A) Schematic representation of the TLK/ASF1 pathway. (B) Immunoblot of TLK and ASF1 in $CD34^{+}$ bone marrow cells from healthy donors (n=3) and AML patient samples (n=8) with indicated mutations. Densitometric analysis of the immunoblot is shown.

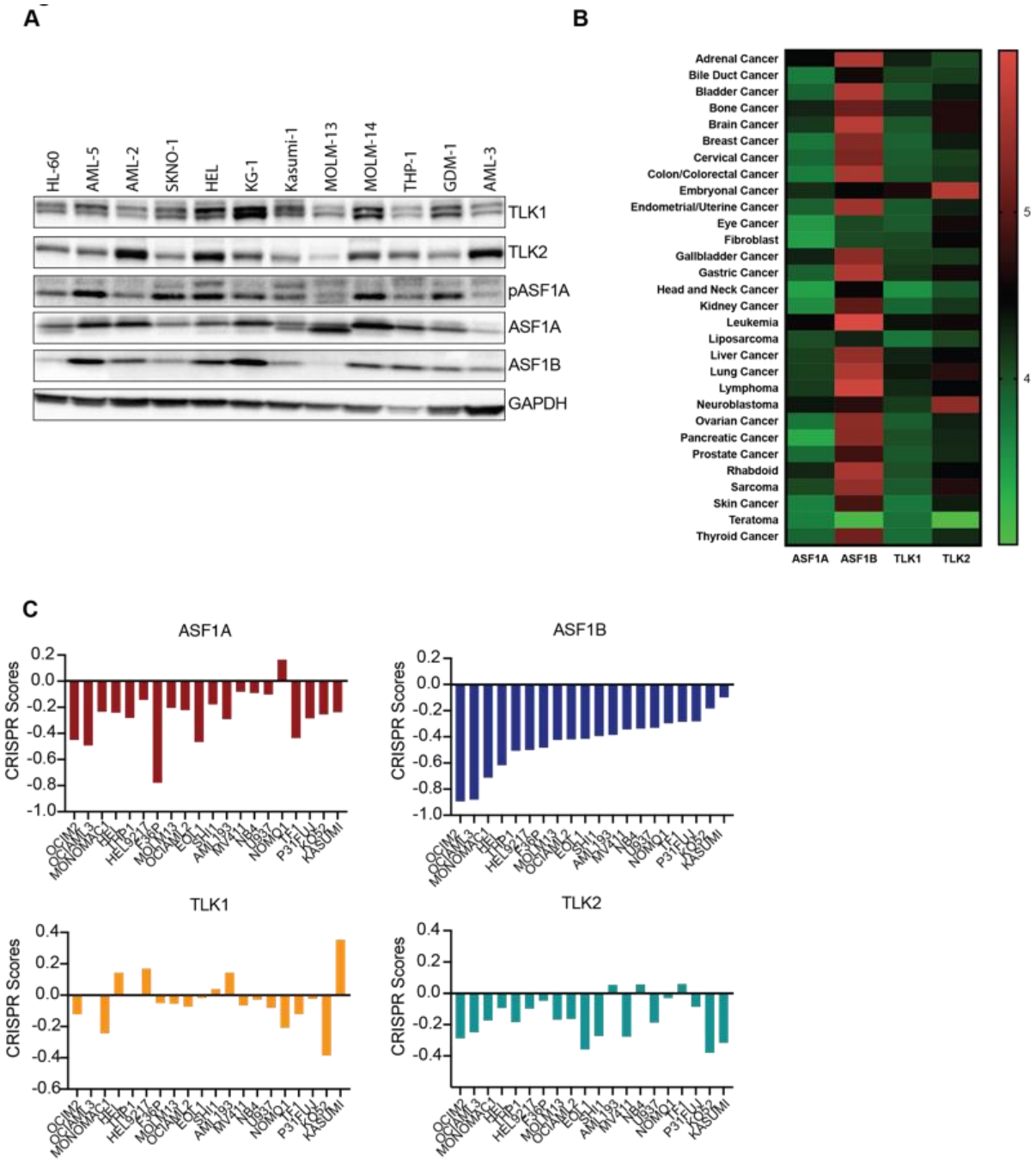

Figure 2.3. Expression of ASF1 and TLK and their dependency in AML cell lines. (A) Immunoblot of TLK/ASF1 levels in AML cell lines. (B) CCLE dataset reveals high expressions of ASF1B across various cancer types. (C) Gene essentiality of TLK and ASF1 in AML cell lines using Genome-wide CRISPR screen from DepMap dataset.

2.1.3 Crosstalk between IL-1β signaling with the TLK-ASF1 pathway drives leukemia progression

Since we have shown that IL-1β promotes AML progression and observed that IL-1β stimulation upregulates *ASF1B* transcript levels in AML progenitors (**Fig. 2.1B**), we wanted to understand whether IL-1β stimulation would also impact the protein levels of ASF1B or ASF1A in AML. We found that IL-1β stimulation led to increased ASF1B levels, but not ASF1A. Although there was no increase in the expression of *TLK1* and *TLK2* transcripts upon IL-1β stimulation, protein levels were upregulated (**Fig. 2.4A, B**).

We next sought to assess how IL-1β regulates the TLK-ASF1 pathway. Our previous study showed that IL-1β promoted AML cell growth through the activation of the downstream p38MAPK; inhibition of p38MAPK reverses IL-1-medicated growth (Carey et al., 2017). To determine whether p38MAPK regulated the TLK-ASF1 pathway in response to IL-1β, we applied small-molecule p38MAPK inhibitors (Doramapimod and Ralimetinib) to IL-1β-treated AML cells. Blockade of p38MAPK abolished IL-1β-induced *ASF1B* expression at mRNA and protein levels, as compared to vehicle treated AML patient samples (**Fig. 2.4**). These results suggested that *ASF1B* is upregulated by IL-1β downstream of p38MAPK. Enrichr analysis (https://maayanlab.cloud/Enrichr/) for the ChEA dataset using genes that are upregulated by IL-1β in AML progenitors suggested that ASF1B may be regulated by several transcription factors (TFs) including E2F4, FOXM1, and MYBL2 (**Fig. 2.5A**). Among these, a E2F family member (E2F1) is a known regulator of *ASF1B* expression (Hayashi et al., 2007) and TCGA analysis indicated that the expression of both *E2F1* and *MYBL2* strongly correlated with *ASF1B*. Similar to what we observed with ASF1 and TLK genes, many AML cell lines showed a high dependency

on *E2F1* and *MYBL2* expression (**Fig. 2.5B, C**) (http://depmap.org/portal/). Accordingly, we found that *E2F1* and *MYBL2* were also upregulated upon IL-1β stimulation in AML progenitors using qPCR analysis (**Fig. 2.5D**). Inhibition of p38MAPK reduces IL-1β-induced expression of *ASF1B* as well as expression of *E2F1* and *MYBL2* expression (**Fig. 2.5D**). Together, these data suggest that IL-1β may upregulate ASF1B through MYBL2 and E2F1 in a p38MAPK dependent manner. Interestingly, IL-1β did not influence the expression of *TLK1* and slightly increased *TLK2* expression at the mRNA level, but both proteins were upregulated at the protein level, suggesting that their translation or stability is influenced by IL-1β through indirect signaling cascades or post-translational regulation.

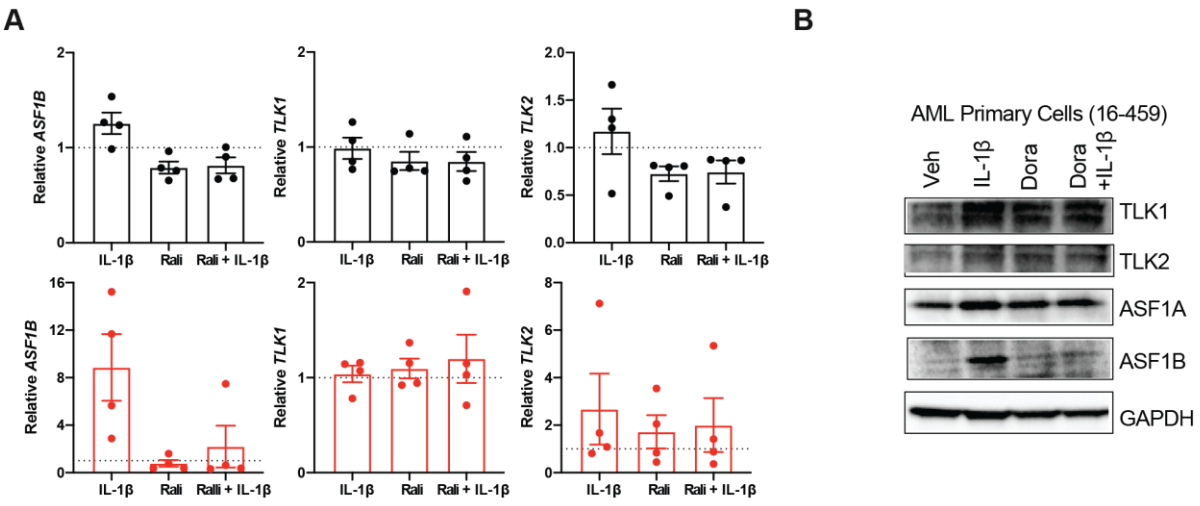

Figure 2.4. TLK and ASF1B expression upon IL-1β stimulation. (A) ASF1B, TLK1, and TLK2 relative mRNA levels by TLDA analysis of healthy (top) and AML (bottom) primary cells upon IL-1β stimulation with and without p38 MAPK inhibitor Ralimetinib (Rali). (B) Immunoblot of AML primary cells treated with or without 10 ng/ml IL-1β in the presence or absence of 500 nM p38 MAPK inhibitor doramapimob (Dora) for 2 days.

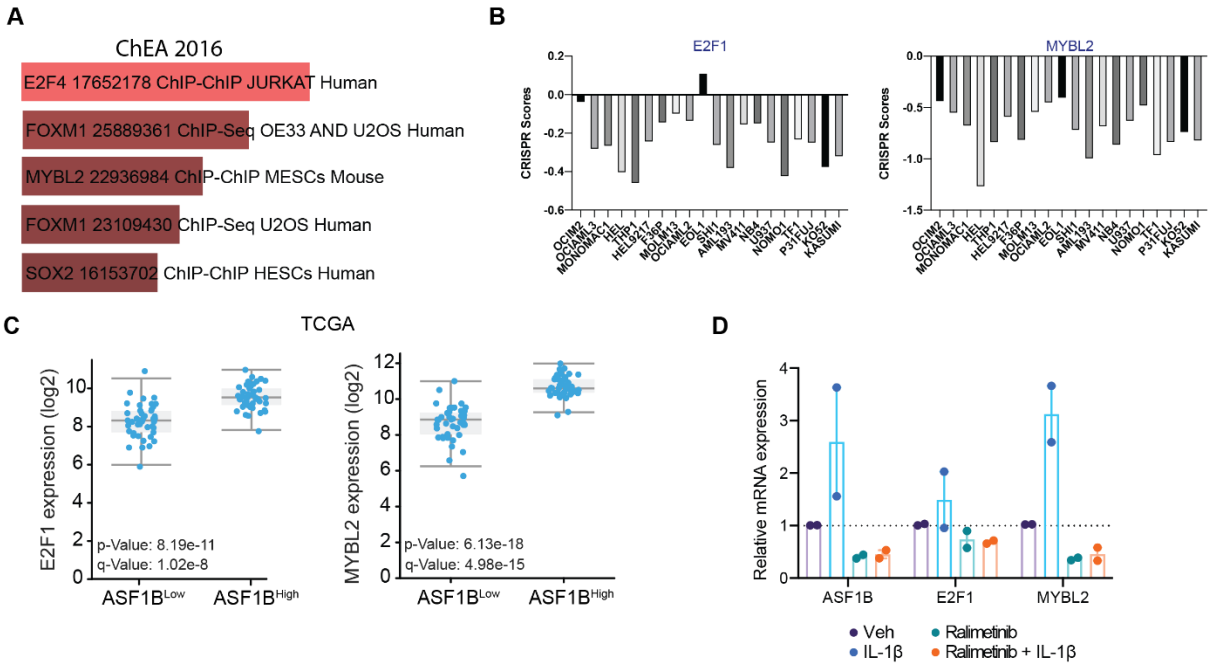

Figure 2.5. IL-1β-mediated transcriptional regulation of ASF1B. (A) Transcription factor (TF) analysis using Erichr ChEA 2016 database showing enrichment of TFs regulating differential expressed genes that are upregulated in AML cells upon IL-1β stimulation compared to IL1-β treated healthy cells (B) Dependency of candidate transcription factors *E2F1* and *MYBL2* in AML cell lines. (C) *E2F1* and *MYBL2* expression in *ASF1B* high and *ASF1B* low patients with AML using TCGA database. (D) *E2F1* and *MYBL2* relative mRNA levels by quantitative PCR of AML primary cells upon IL-1β stimulation with and without p38 MAPK inhibitor (Ralimetinib).

2.1.4 Absence of ASF1 suppresses the growth and leukemia burden in AML

To determine the role of ASF1 in AML, we depleted *ASF1A*, *ASF1B*, or both, using doxycycline (dox) inducible, small hairpin RNAs (shRNAs) in MOLM-14 cells, which harbor a FLT3-ITD mutation, one of the most common mutations in AML (**Fig. 2.6A, B**). We observed second smaller size ASF1A bands upon *ASF1B* knockdown, suggesting phosphorylation of ASF1A and its stability may be affected by ASF1B level. Depletion of ASF1A or ASF1B impaired MOLM-14 cell growth (**Fig. 2.6D**), while non-targeting hairpins did not (**Fig. 2.8A, B**). The effect of combined knockdown of both ASF1A and ASF1B was similar to knockdown of ASF1B alone, suggesting that ASF1B may compensate for loss of ASF1A in ASF1A-depleted cells (**Fig. 2.6D**). Cell cycle analysis demonstrated that a proportion of cells accumulated at G0/G1 phase, accompanied by decreased S and G2/M phase populations upon ASF1A or ASF1B knockdown, suggesting impaired progression from G0/G1 to S phase or cell cycle exit (**Fig. 2.6E**). Consistent with proliferative defects of cell cycle arrest, the depletion of ASF1A, ASF1B, or both, resulted in a 52%, 84%, and 82% reduction in colony formation assay compared to controls (**Fig. 2.6F**). To examine the effect of ASF1 depletion *in vivo*, our laboratory has xenografted MOLM-14 cells expressing shASF1A (RFP^+), shASF1B (GFP^+), and shASF1A+B (GFP^+RFP^+) into NOD-SCID $IL2R^{-/-}$(NSG) mice and assessed their leukemic burden (**Fig. 2.7A).** Using RFP/GFP^+ and cell surface markers $CD13^+CD33^+$ and $CD15^+$, we found that ASF1 knockdown reduced the leukemic burden by 82% for ASF1A, 95% for ASF1B, and 82% for ASF1A+B in the bone marrow compared with controls (**Fig. 2.7B, C**). Spleen weight of the doxycycline-treated group was reduced 69% for ASF1A, 66% for ASF1B, and 59% for ASF1A+B groups compared with controls (**Fig. 2.7D**). MOLM-14 cells expressing non-

targeting shRNA (shNT16 or shNT17) were xenografted into NSG mice and we observed no significant differences in leukemic burden in doxycycline-treated and untreated groups (**Fig. 2.8 C, D**). Collectively, these results indicated that both ASF1A or ASF1B can potentiate AML cell growth and that targeting either ASF1A or ASF1B was sufficient to impair AML growth.

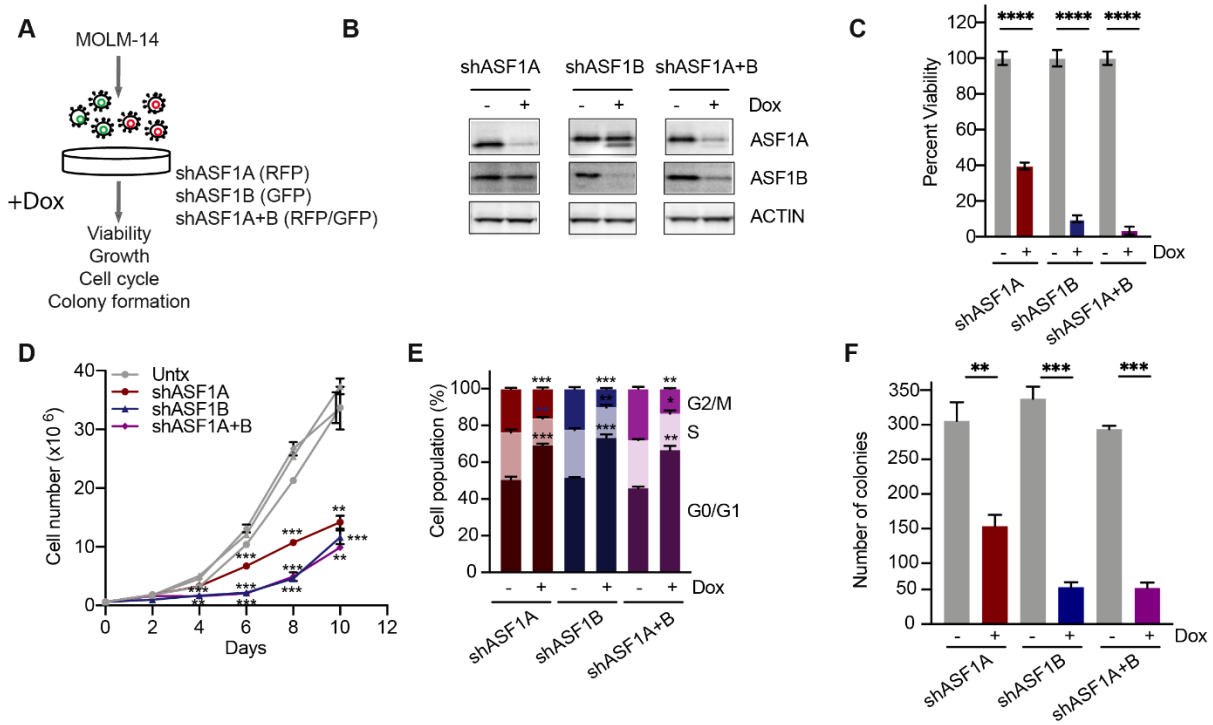

Figure 2.6. Reduced expression of ASF1 suppresses *in vitro* AML growth. (A) schematic representation of doxycycline inducible shRNA model targeting ASF1A, ASF1B, or both ASF1A+ASF1B in MOLM-14 cells. (B) MOLM-14 cells were treated with 1 μg/ml doxycycline to induce knockdown for 6 days. The effect of knockdown was measured by immunoblotting analysis. shRNA expressing cells were kept in doxycycline containing media throughout and the effect of knocking down ASF1A, ASF1B, or both ASF1A+ASF1B on (C) cell viability was measured by colorimetric (MTS) assays following doxycycline-induced knockdown for 6 days, (D) cell growth overtime was indicated by cell counts. shRNA expressing cells were kept in doxycycline containing media throughout, (E) cell cycle analysis using propidium iodide and flow cytometry, and (F) colony formation by plating cells in methylcellulose-based medium.

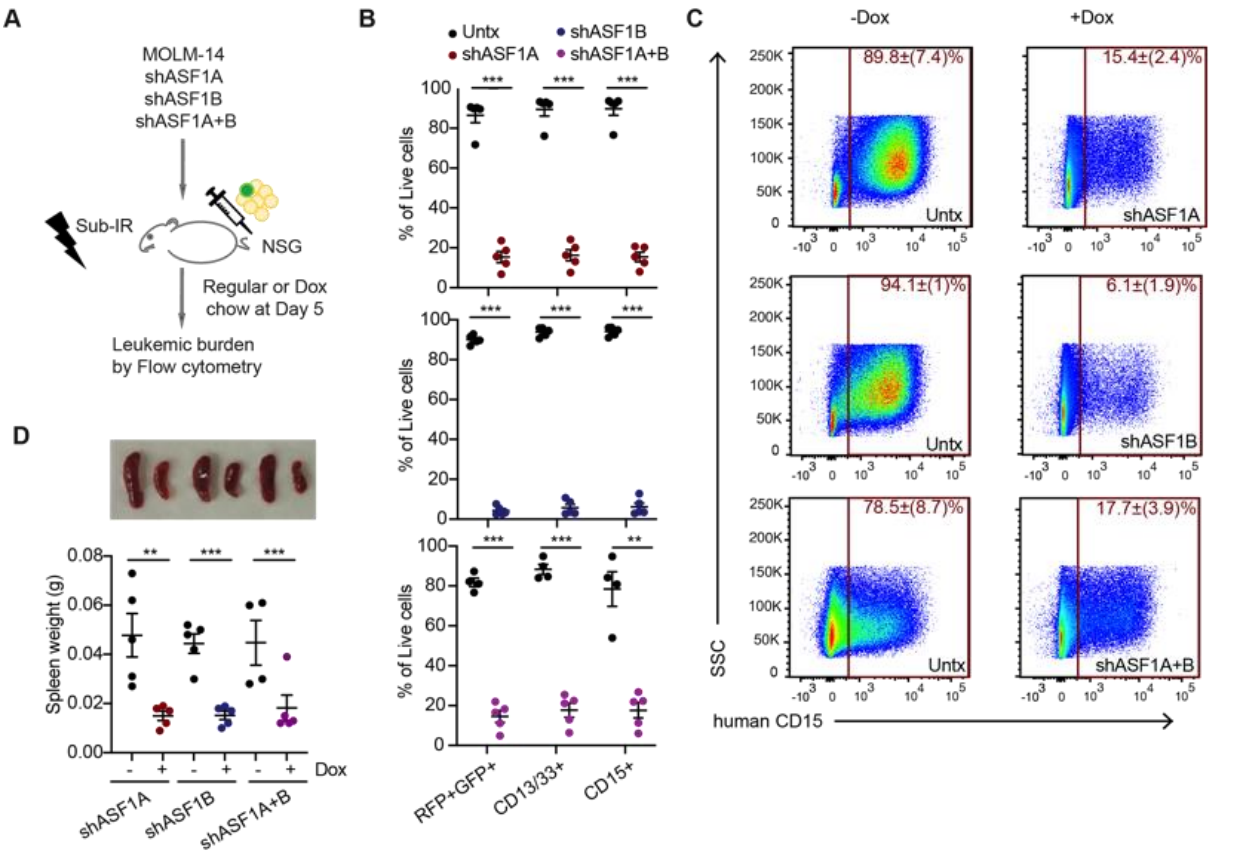

Figure 2.7. Reduced expression of ASF1 suppresses *in vivo* AML growth and leukemia burden using human cells. (A) MOLM-14 cells expressing shASF1A, shASF1B or both were xenografted into sublethally irradiated NSG mice, which were randomly divided in two groups with or without 625 mg/kg doxycycline chow. All the mice were sacrificed 18 days post treatment (n =4-5/group). (B, C) Leukemic burden was determined by GFP and/or RFP positivity, human CD13/CD33, and CD15 levels using flow cytometry. (D) Spleen weight and representative spleens were shown from each group. Data are expressed as means ± SEM. * P < 0.05, ** P < 0.01, *** P < 0.001.

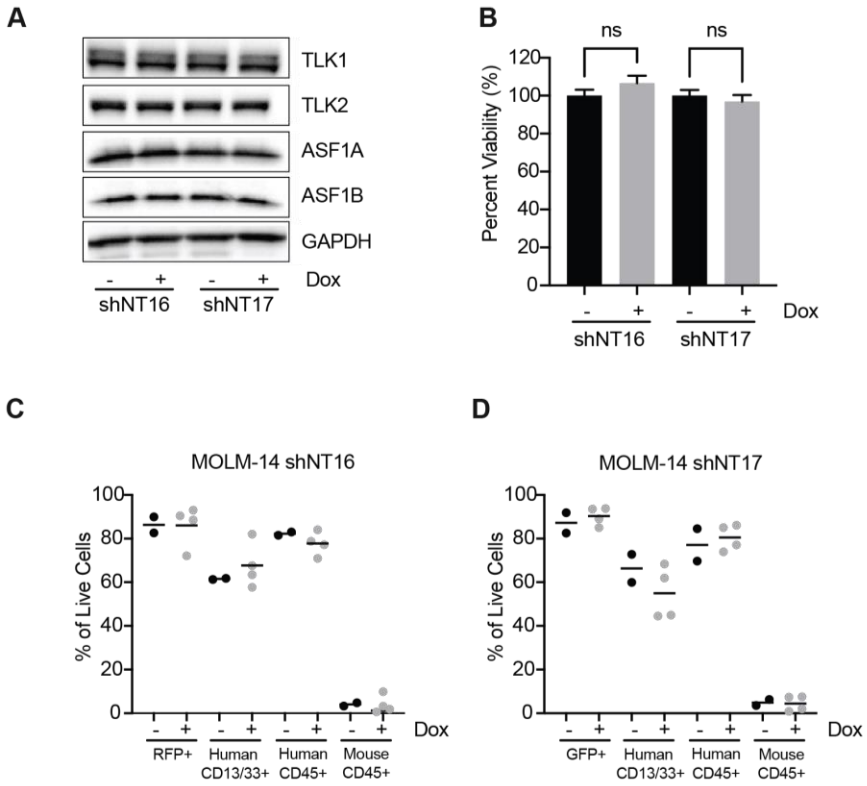

Figure 2.8. The effect of non-targeting shRNA controls *in vitro* and *in vivo* on the viability of AML cells and leukemia burden using human cells in xenograft model. (A) Immunoblot of MOLM-14 cells expressing non-targeting shRNAs NT16 (RFP expressing) and NT17 (GFP expressing). (B) Cell viability by colorimetric (MTS) assays following doxycycline-induced knockdown on day 6 (C, D) MOLM-14 cells expressing shNT16 or shNT17 were xenografted into sublethally irradiated NSG mice, which were randomly divided in two groups with or without doxycycline chow. All the mice were sacrificed 18 days post treatment. Leukemic burden was determined by GFP or RFP positivity, human CD13/CD33, and CD15 levels using flow cytometry. Data are expressed as means ± SEM. * $P < 0.05$, ** $P < 0.01$, *** $P < 0.001$.

2.1.5 ASF1B is a mediator of IL-1β-driven AML progression

To test the hypothesis that IL-1β promotes AML progression by regulating the expression of *ASF1B*, we used a murine bone marrow transplantation model of AML driven by an oncogenic fusion protein, MLL-ENL (Zuber et al., 2009). MLL-ENL is one of the most common AML subtypes. We transduced wild-type bone marrow cells with retrovirus expressing MLL-ENL and GFP, along with retrovirus expression of ASF1B and mCherry, or mCherry alone as an empty vector control. Sorted double positive cells were subsequently transplanted into lethally irradiated recipient mice. IL-1β level is elevated in the blood and bone marrow of patients with AML (Carey et al., 2017). To model how inflammation drives AML progression, we treated recipient mice with IL-1β or vehicle daily via intraperitoneal injection 2 weeks post-transplantation. Differential blood counts and GFP/RFP expression were analyzed every week in peripheral blood to determine the degree of engraftment (**Fig. 2.9A**). We found that mice treated with IL-1β succumbed to the disease rapidly (median survival = 64 days, range = 31-80 days), compared to the mice treated with vehicle (median survival = 85 days, range = 63-112 days, $P = 0.028$). Notably, ectopic ASF1B expression shortened survival (median survival = 62 days, range = 36-84 days, $P = 0.019$), mimicking IL-1β-mediated AML progression. Additionally, ASF1B overexpression with IL-1β treatment also accelerated disease progression (median survival = 57 days, range = 41-72 days, $P = 0.005$) (**Fig. 2.9B**). At 5-7 weeks post-transplant, we observed higher leukemic cells in the peripheral blood of IL-1β-treated ASF1B-overexpressing recipients (**Fig. 2.9C**). At the terminal-stage, spleen and liver weights were comparable between each group (**Fig. 2.9D**) and all the mice showed myeloid expansion of leukemic cells in the bone marrow (**Fig. 2.9E**). Taken together,

these results suggest that IL-1β treatment or ASF1B overexpression promoted myeloid expansion and leukemia progression.

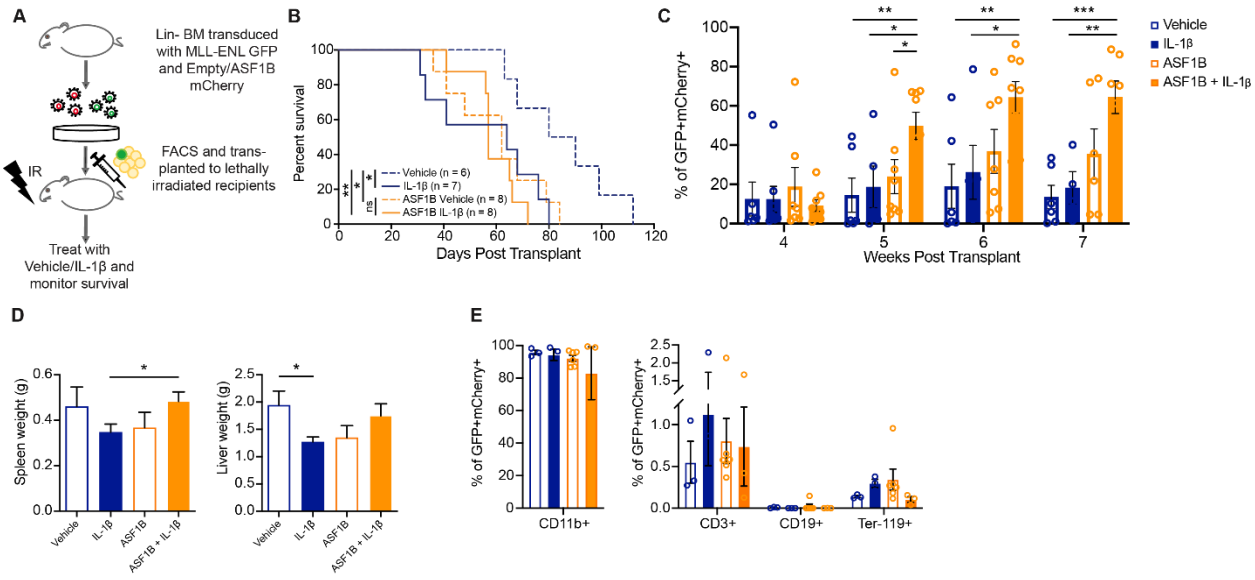

Figure 2.9. ASF1B potentiates IL-1β-driven AML progression in a murine model of leukemia. (A) A schematic representation of ASF1B overexpression in a murine AML bone marrow transduction/transplantation model. Lineage depleted wild-type bone marrow cells were transduced with MSCV-IRES-mCherry or MSCV-IRES-ASF1B-mCherry and MSCV-IRES-MLL-ENL-GFP constructs. 10,000 sorted mCherry^{+}GFP^{+} cells were injected into lethally irradiated C57BL/6 recipients. Mice were monitored daily and euthanized when they appeared moribund or showed signs of sickness. (B) Kaplan Meier survival curve of mice following treatment with 0.25 μg IL-1β (C) Percentage of leukemic cells in peripheral blood overtime by flow cytometry. (D) Spleen and liver weights at endpoint from ASF1B-MLL-ENL overexpression bone marrow transplantation model (BMT). (E) Immunophenotyping at endpoint from ASF1B-MLL-ENL overexpression BMT. or vehicle. Log rank test is used for statistical analysis. * $P < 0.05$, ** $P < 0.01$, *** $P < 0.001$.

To further evaluate whether ASF1B plays a role in IL-1-mediated AML progression, we performed complementary studies using *Asf1b*$^{-/-}$ mice. To determine whether *Asf1b* deletion suppresses leukemogenesis and IL-1β-mediated progression *in vivo*, we transplanted *Asf1b*$^{+/+}$, *Asf1b*$^{+/-}$, and *Asf1b*$^{-/-}$ cells expressing MLL-ENL and GFP into lethally irradiated recipients (**Fig. 2.10 A**). Heterozygous and homozygous *Asf1b* deletion (median survival = 68 days and 67 days, range = 58-84 days and 60-84 days, respectively) extended survival of leukemic mice compared to wild-type mice (median survival = 62 days, range = 47-68 days, respectively) (**Fig. 2.10 C**). Delayed progression were also observed in the peripheral blood of *Asf1b*$^{+/-}$, and *Asf1b*$^{-/-}$ recipients at 8 weeks post-transplantation (**Fig. 2.10 E**). Notably, deletion of *Asf1b* also attenuated IL-1β-mediated leukemia progression in the *Asf1b*$^{-/-}$ recipients versus the *Asf1b*$^{+/+}$ recipients (**Fig. 2.10 C**) (median survival = 63 days versus 47 days, range = 53-67 days and 40-61 days, respectively). Slight reduction of spleen weight and liver weight was observed in *Asf1b*$^{-/-}$ recipients and smaller liver size in *Asf1b*$^{+/-}$ recipients (**Fig. 2.10 F**). All groups exhibited myeloid expansion of leukemia cells at terminal stage (**Fig. 2.10 G**) and reduced disease burden was observed in *Asf1b*$^{-/-}$ recipients with and without IL-1β treatment. Additionally, we assessed the impact of ASF1B depletion in normal hematopoiesis. Interestingly, we observed no significant difference in differential blood counts of *Asf1b*$^{+/+}$, *Asf1b*$^{+/-}$, and *Asf1b*$^{-/-}$ mice (**Fig. 2.11A**). Accordingly, flow cytometry analysis of bone marrow cells showed no significant difference in cell lineage markers or stem and progenitor cell populations (**Fig. 2.11B**), suggesting that there are no major hematopoietic defects in ASF1B-deficient cells. Overall, these data suggest that ASF1B is one of the mediators for IL-1β-driven AML progression and the suppression of ASF1B delayed the leukemia

progression at steady state and under inflammatory stress while healthy hematopoiesis is not impacted by ASF1B deletion.

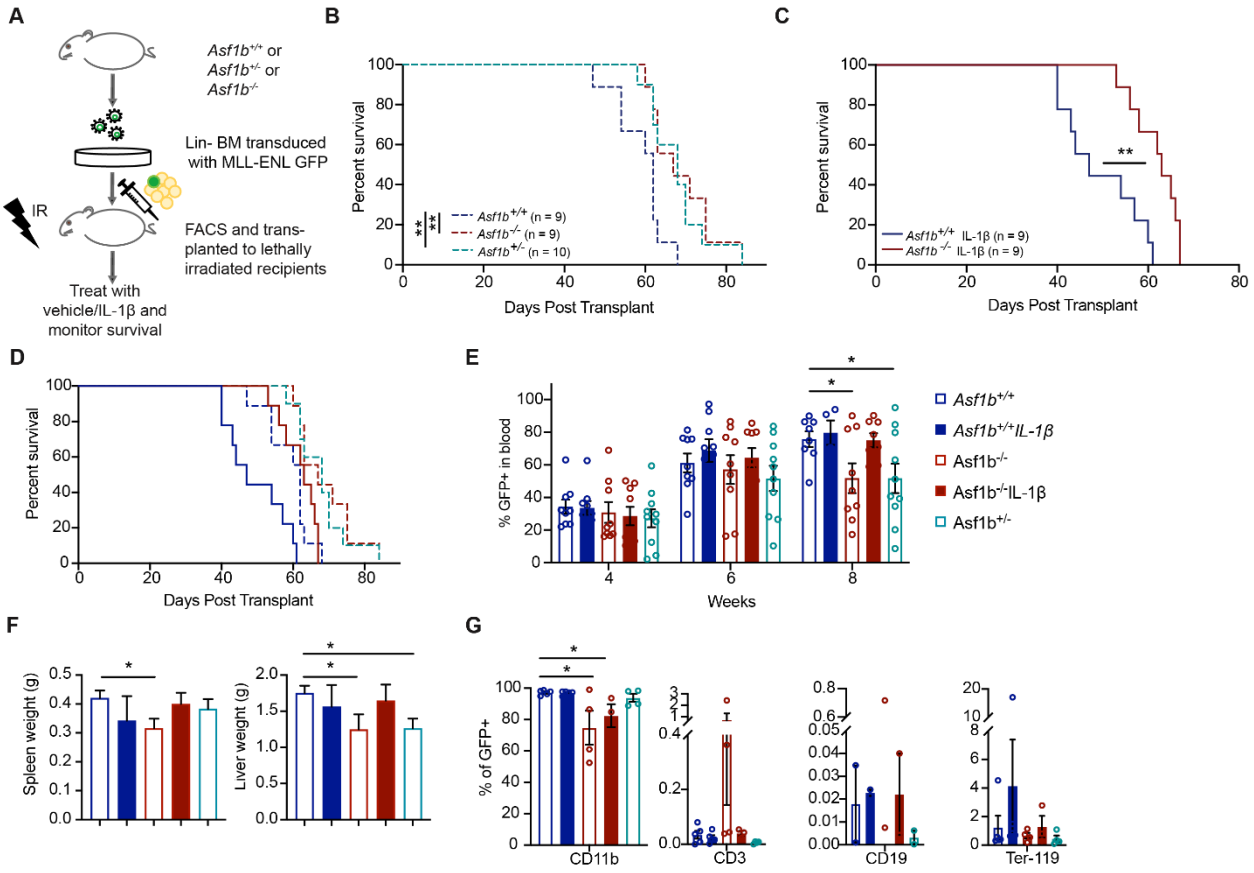

Figure 2.10. Absence of ASF1B attenuates the leukemia progression. (A) A schematic representation of a murine AML bone marrow transduction/transplantation model to study effect of ASF1B deletion on leukemia progression. Lineage depleted *Asf1b*$^{+/+}$, *Asf1b*$^{+/-}$, *Asf1b*$^{-/-}$ bone marrow cells were transduced with MSCV-IRES-MLL-ENL-GFP retrovirus. After 48 hrs of transduction 25,000 sorted GFP+ cells were injected into lethally irradiated recipient mice. (B, C) Kaplan Meier survival curve of mice following treatment with 0.25 μg IL-1β or vehicle. Log rank test is used for statistical analysis. * P < 0.05, ** P < 0.01, *** P < 0.001. (D) Combined survival curves from B and C. (E) Percentage of leukemic cells in peripheral blood overtime from *Asf1b* deletion BMT. (F) Spleen and liver weights and (G) immunophenotyping at endpoint from *Asf1b* deletion BMT.

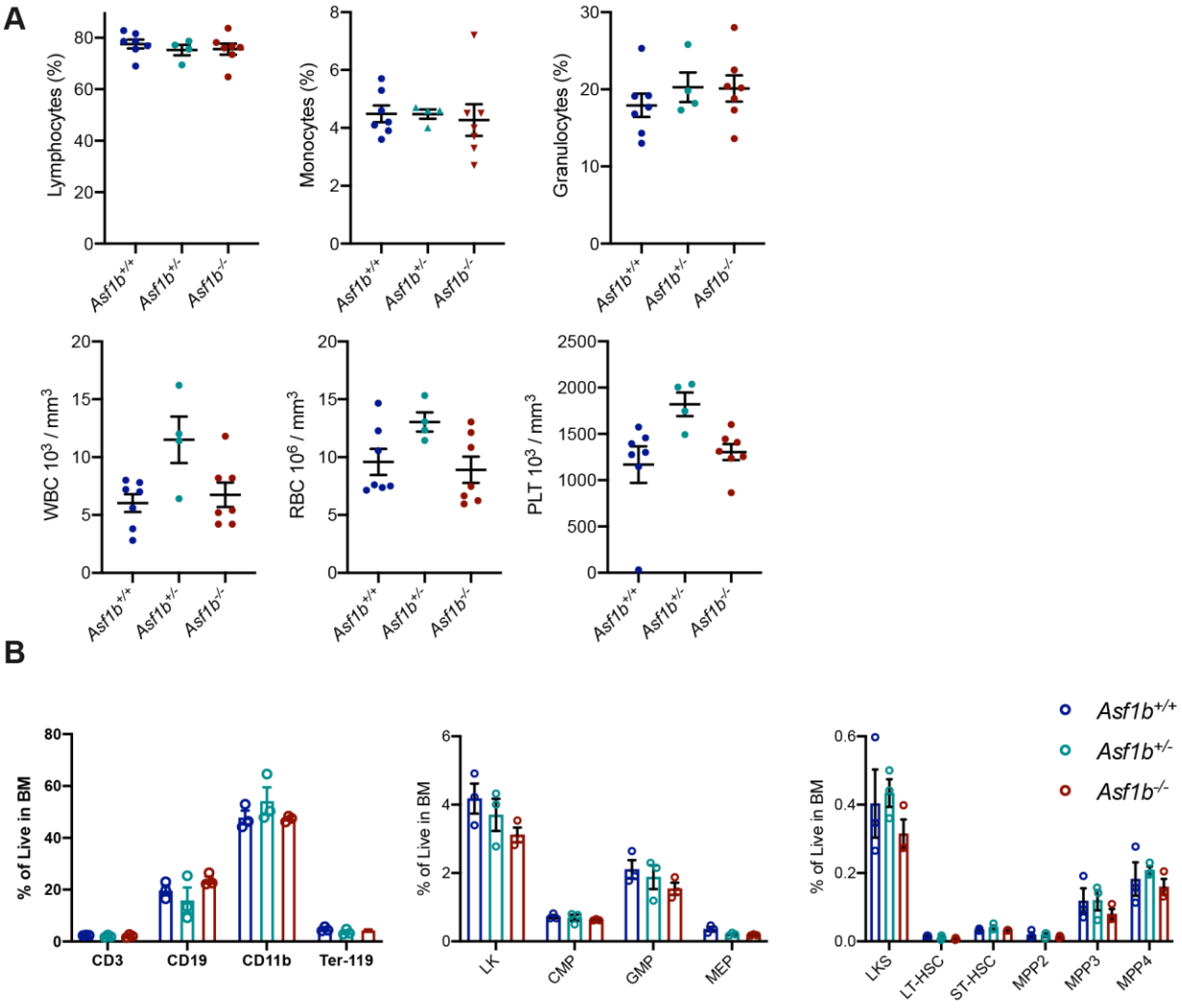

Figure 2.11. Deletion of ASF1B is dispensable for normal hematopoiesis. (A) Complete blood counts in *Asf1b*$^{+/+}$, *Asf1b*$^{+/-}$, and *Asf1b*$^{-/-}$ mice before transplantation. WBC, white blood cells; RBC, red blood cells; PLT, platelets. (B) The distribution of stem and progenitor cells in the bone marrow of *Asf1b*$^{+/+}$, *Asf1b*$^{+/-}$, and *Asf1b*$^{-/-}$ mice was measured by flow cytometry.

Chapter 3: Role of TLK in AML progression

3.1 Results

3.1.1 Genetic targeting of TLK1 and TLK2 suppresses AML growth and leukemic burden

ASF1A and ASF1B are known substrates of TLKs, which are promising targets for various cancer types (Klimovskaia et al., 2014; Segura-Bayona and Stracker, 2019). To examine whether TLK1 and TLK2 are also required for AML cell growth and survival, we used two independent shRNA hairpins to knock down *TLK1*, *TLK2*, or both genes, in MOLM-14 cells. We confirmed the knockdown efficiency by western blotting of protein levels and also observed reduced phosphorylation of ASF1A upon knockdown of either TLK1, TLK2 or both. There was no significant change in total ASF1A and ASF1B levels (**Fig. 3.1A, B**). Similar to ASF1 knockdown and consistent with their role in regulating ASF1 function, depletion of TLK1, TLK2, or both, resulted in a significant reduction of AML cell viability, cell expansion, colony formation ability (**Fig. 3.1C, D, F**). TLK1 or TLK2 depletion alone modestly altered cell cycle and depletion of both TLKs arrested cell cycle at G0/G1 (**Fig. 3.1E**).

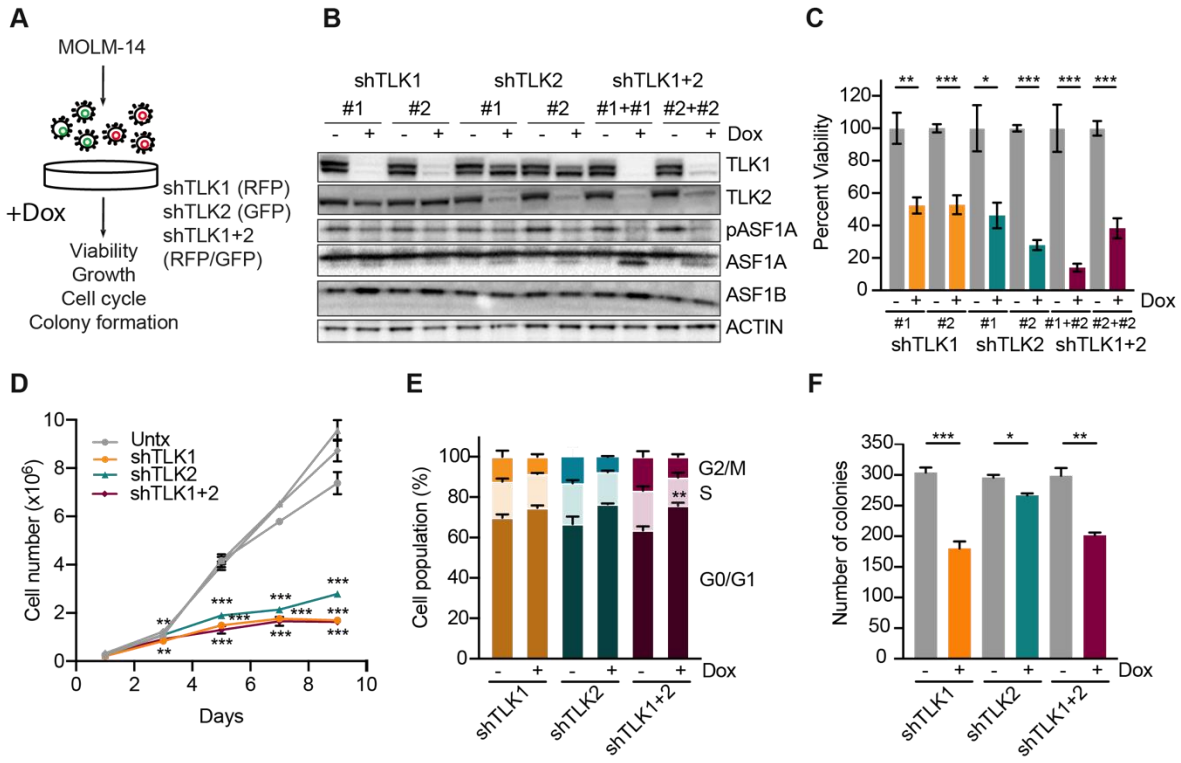

Figure 3.1. Reduced expression of TLKs suppresses *in vitro* and *in vivo* AML growth and leukemia burden using human cells. (A) A schematic representation of shRNA model targeting TLK1, TLK2, or both TLK1+TLK2 in MOLM-14 cells. (B) MOLM-14 cells were treated with 1 μg/ml doxycycline to induce knockdown for 6 days. The effect of knockdown was measured by immunoblotting analysis. The effect of knocking down TLK1, TLK2, or both TLK1+TLK2 on (C) Cell viability by colorimetric (MTS) assay following doxycycline-induced knockdown for 6 days, (D) cell growth overtime was indicated by cell counts, (E) cell cycle analysis using propidium iodide and flow cytometry, and (F) colony formation ability by plating cells in methylcellulose-based medium. Data are expressed as means ± SEM. * $P < 0.05$, ** $P < 0.01$, *** $P < 0.001$.

3.1.2 DNA damage pathway is altered upon TLK and ASF1 knockdown

Since the TLK-ASF1 pathway is involved in diverse cellular processes, such as cell cycle progression and the DNA damage response, we next examined signaling mediators of these pathways. Upon both ASF1A and ASF1B depletion, we observed an increase in H2AX phosphorylation at S139 (γ-H2AX), a marker of DSBs, compared to individual depletion of ASF1A or ASF1B or non-targeting control cells (**Fig. 3.2**). Further, compared to non-targeting control cells, other DNA damage and replication stress markers p-p53 (Ser 15), pRPAS4/S8, and pChk2 (Thr 68) were elevated in ASF1A, ASF1B, and ASF1A+B KD cells, which had greater responses than single ASF1A or ASF1B knockdown. Both p53 and p21 protein levels were elevated in ASF1 KD cells, indicating that the G1/S cell cycle checkpoint was activated to block S-phase entry. In TLK-depleted cells, we found depletion of both TLK1 and TLK2 increased γ-H2AX levels. Further, the combined depletion of TLK1 and TLK2 slightly increased on phosphorylation of p53, RPAS4/S8, and CHK2, compared to depletion of TLK1 or TLK2 alone and non-targeting control (**Fig. 3.2**). Total p21 and p53 levels were also increased upon TLK1+2 knock down as compared to nontargeting controls, suggesting TLK and ASF1-depleted cells may have many overlapping downstream signaling changes.

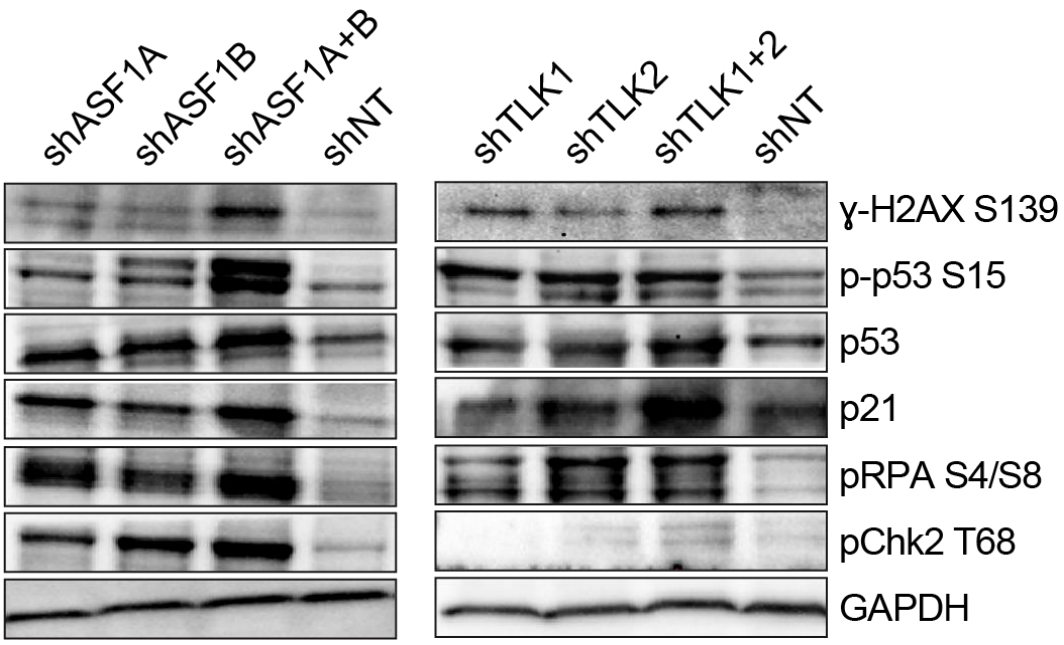

Figure 3.2. DNA damage pathway is altered upon TLK and ASF1 knockdown. Immunoblotting of proteins involved in cell cycle and replication stress in MOLM-14 cells upon TLK and ASF1 knockdown.

3.1.3 TLK2 kinases as mediators of IL-1β-driven AML progression

We showed primary AML samples have higher protein levels of TLK1 and TLK2, with TLK2 levels more dramatically changed than TLK1 in AML compared to healthy cells (**Fig. 2.2B**). Additionally, combined knockdown of TLK1 and TLK2 did not confer much stronger growth defects compared to TLK2 knockdown alone (**Fig. 3.1C, D**). Depmap analysis showed more dependency on TLK2 compared to TLK1 for the fitness of AML cells (**Fig. 2.3C**). Therefore, we asked whether TLK2 loss would impair AML progression. Since complete deletion of *Tlk2* is embryonically lethal, we crossed *Tlk2*$^{f/f}$ mice (Segura-Bayona et al., 2017) with *Vav-Cre* mice to conditionally delete *Tlk2* in hematopoietic cells. Depletion of *Tlk2* was confirmed by qRT-PCR (Transnetyx). Immunopheotyping of *Tlk2*$^{+/+}$, *Tlk2*$^{+/-}$, and *Tlk2*$^{-/-}$ mice showed that *Tlk2* deletion mice had slightly lower B-cell numbers but, other cell types were comparable, including stem and progenitor cell populations (**Fig. 3.3**).

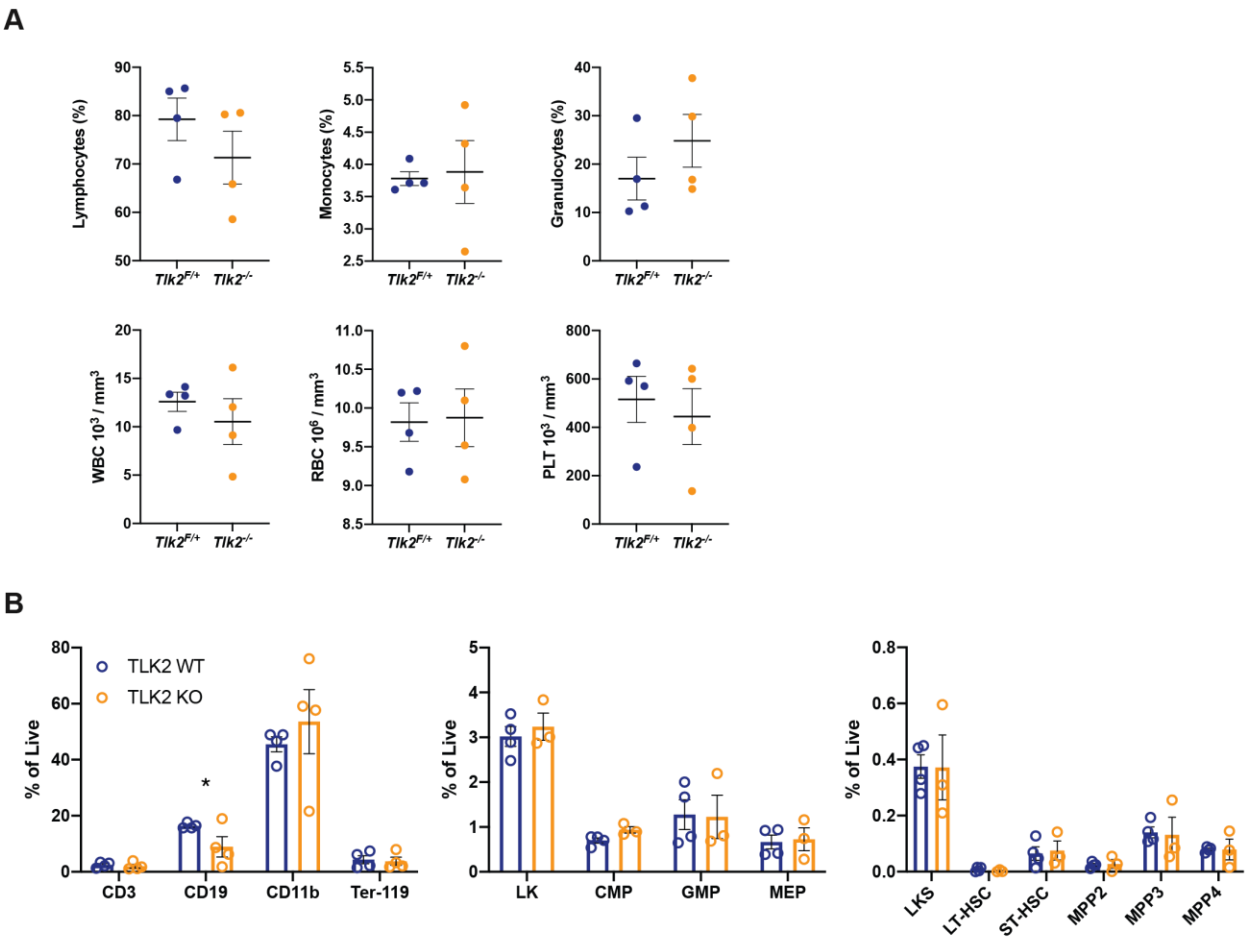

Figure 3.3. Immunophenotyping of TLK2 mice (A) Complete blood counts in *Tlk2*$^{+/+}$, *Tlk2*$^{+/-}$, and *Tlk2*$^{-/-}$ mice. (B) Immunophenotyping of *Tlk2*$^{+/+}$, *Tlk2*$^{+/-}$, and *Tlk2*$^{-/-}$ mice in bone marrow and the distribution of stem and progenitor cells.

Using the MLL-ENL murine model of AML (**Fig. 3.4A**), heterozygous and homozygous deletion of *Tlk2* (median survival = 138 days and 187 days) significantly extended the survival compared to wild type recipients (median survival = 84 days). These data suggest that TLK2 is haploinsufficient for AML progression and even a 50% reduction in expression or activity might improve the survival of the patients **(Fig. 3.4B)**, Further, *Tlk2* depletion significantly extended the survival of IL-1β-treated mice compared to IL-1β-treated WT mice (median survival = 110 days versus 75 days, ranges = 87-229 days and 61-87 days, respectively, *P* = 0.0327) **(Fig. 3.4B)**. The percentage of GFP+ cells from *Tlk2*+/+ and KO were comparable at 3 weeks post-transplant and their homing efficiency to the bone marrow were similar **(Fig. 3.4C, D**), indicating that TLK2 deletion does not impair the engraftment ability. At the endpoint, flow cytometry analyses of bone marrow cells showed that GFP+ leukemic cells are mostly myeloid cells and were comparable between each group (**Fig. 3.4E, F)**.

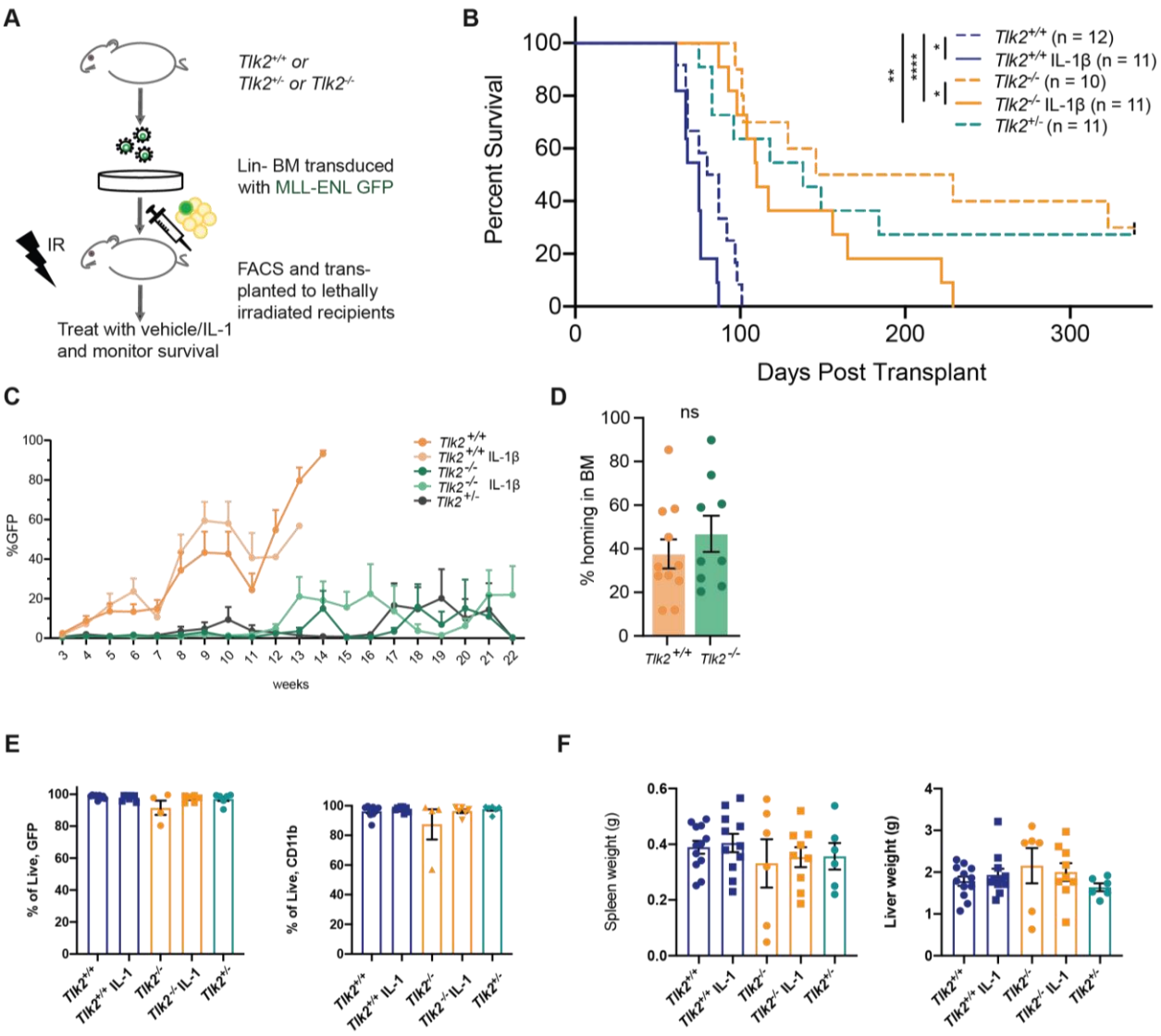

Figure 3.4. Absence of TLK2 attenuates leukemia burden and IL-1-driven AML progression in a murine model of leukemia. (A) A schematic representation of a murine AML bone marrow transduction/transplantation model to study effect of TLK2 deletion on leukemia progression. Lineage depleted *Tlk2*$^{+/+}$, *Tlk2*$^{+/-}$, *Tlk2*$^{-/-}$ bone marrow cells were transduced with MSCV-IRES-MLL-ENL-GFP retrovirus. After 48 hrs of transduction 15,000 sorted GFP+ cells and 250,000 supporting cells were injected into lethally irradiated recipient mice. (B) Survival curve of mice following treatment with 0.25 μg IL-1β or vehicle is shown. Log rank test is used for statistical analysis. (C) Percentage of leukemic cells in peripheral blood overtime by flow cytometry. (D) The percent of transplanted CFSE+ cells that homed to the bone marrow. (E) Percentage of leukemic cells and immunophenotyping at endpoint in the bone marrow from *Tlk2* deletion BMT. (F) Spleen and liver weights at disease endpoint from *Tlk2* deletion BMT. *P < 0.05, ** P < 0.01, *** P < 0.001.

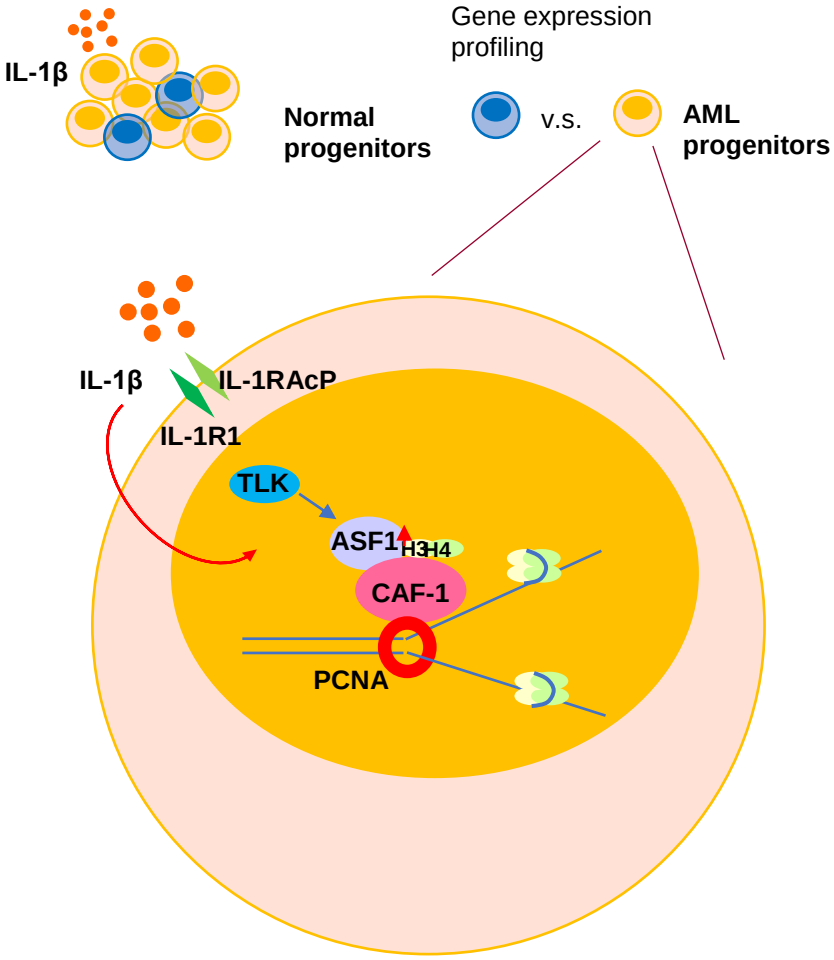

Figure 3.5. Schematic showing role of TLK/ASF1 in IL-1β mediated AML progression. ASF1B is upregulated in AML progenitors upon IL-1β-mediated inflammatory stress. TLK or ASF1 deletion mitigates AML cell growth while sparing healthy hematopoiesis. Targeting ASF1B or TLK2 suppresses IL-1β-driven AML progression by impacting cell cycle and DNA damage responses.

Chapter 4: Discussion and Future Directions

Despite recent improvements of targeted inhibitors and combination therapies, the 5-year survival rate for patients with AML remains low (~25%). In part, this is due to the rapid emergence of drug resistant mutations in leukemic cells (McMahon et al., 2019; Nechiporuk et al., 2019). Additionally, the bone marrow microenvironment exerts inflammatory stress and becomes growth-permissive to malignant clones over healthy cells. This demands an improved understanding of disease biology and the identification of novel therapeutic targets that are active across AML genetic subtypes. In this study, we showed that aberrant IL-1β signaling drives AML progression through the upregulation of the TLK-ASF1 histone chaperone pathway. Knockdown of either ASF1 or TLK family members impaired cell growth and survival in both *in vitro* and *in vivo* models of AML, representing multiple genetic subtypes of AML. Further, we found that depletion of ASF1B or TLK2 impaired IL-1β-driven AML progression in a murine model, suggesting that the TLK-ASF1 pathway represents a novel therapeutic target for AML. Previously it was shown that different isoforms of TLKs (TLK1 and TLK2) and ASF1s (ASF1A and ASF1B) may contribute to cancer initiation, development, and progression in a variety of cancer types through distinct mechanisms (Kim et al., 2016; Li et al., 2020; Yang et al., 2018). Additionally, high ASF1B or TLK2 expression is associated with poor patient outcome in subsets of patients with breast cancer (Corpet et al., 2011; Lee et al., 2018).

Despite numerous studies implicating the ASF-TLK pathway in cancer, its role in leukemia and hematopoiesis has not been previously examined in detail. Our results indicate that heterozygous or complete deletion of either ASF1B or its regulator, TLK2, delay AML progression at steady state and under IL1β-mediated inflammatory stress. Previous work

showed that, overexpression of CHAF1B, a subunit of the CAF-1 histone chaperone complex that interacts with ASF1B, promoted AML progression in a murine model of MLL-AF9 positive AML (Volk et al., 2018). As CAF1 is predominantly involved in replication-dependent histone deposition, these results are consistent with an enhanced dependence of AML on the TLK-ASF1 pathway. Previous work in breast cancer that reported ASF1A expression in both proliferating and quiescent breast cancer cells, while ASF1B was only expressed in proliferating cells and its knockdown impacted colony formation (Corpet et al., 2011). However, in our *in vivo* leukemia model, ASF1B deletion was unable to completely eliminate the disease, suggesting that ASF1A, or other molecular targets including CAF1, may contribute to AML progression in the absence of ASF1B. This is consistent with ASF1A depletion having a significant impact on AML growth *in vitro* (**Fig. 2.6**), and with previous observations that ASF1A depletion caused growth arrest in hepatocellular carcinoma (HCC) and prostate cancer cells (Wu et al., 2019). Despite the similar outcomes observed with ASF1B and CAF1 in leukemia, recent work suggested that loss of these pathways may play a pro-metastatic role in some cancers. For example, signaling through TGF or ERK pathways reduced levels of histone H3 and CAF-1, resulting in increased chromatin accessibility that promoted genes associated with the epithelial-mesenchymal transition and aggressive traits (Gomes et al., 2019). Thus, the dependency and therapeutic potential of CAF1 and ASF1 may be cancer type specific or stage dependent.

Elevated ASF1B or TLK2 in breast cancer was proposed to provide a growth advantage for cancer cells via enhanced cell cycle progression and tolerance of replication stress and DNA damage (Kim et al., 2016; Yang et al., 2018) and elevated TLK1 or TLK2

expression correlated with poor prognosis in several other cancer types using multivariate analyses (Lee et al., 2018). In contrast to previous work in osteosarcoma cells that observed pronounced replication stress and DNA damage following TLK1/2, but not ASF1A/B depletion (Lee et al., 2018), we observed a stronger DNA damage response following ASF1 depletion than TLK depletion in AML (**Fig. 3.2**). This may indicate that additional targets of TLK activity, such as the DNA repair factor RAD9 or the kinase NEK1, may play a role in the phenotypes (Kelly and Davey, 2013; Singh et al., 2020). It could also reflect specific functions of ASF1 that are not dependent on TLK activity, such as the role of ASF1A in NHEJ-mediated repair (Lee and Dutta, 2021; Lee et al., 2017). This is in contrast to a recent study that showed significantly increased levels of γ-H2AX and pRPA-S4/S8 while siASF1(a+b) did not induce strong replication stress (RPA pS33) and DNA damage responses (Lee et al., 2018). ASF1A/B knockdown reduced expression of p53/p21, suggesting that they may function differently than TLK-depleted cells (**Fig. 3.2**). In HCC and prostate cancer cells (Wu et al., 2019), p53/p21cip1 expression was increased upon ASF1A depletion.

TLK depletion enhanced chromatin accessibility and provoked cGAS-STING-dependent sterile inflammatory responses in multiple cancer cell types *in vitro* (Segura-Bayona et al., 2020). In addition, ASF1A depletion sensitized non-small cell lung cancer cells to PD-1 immunotherapy by upregulating inflammatory genes associated with T-cell activation, including TNFα (Li et al., 2020). However, to our knowledge, prior studies have not examined the role of the TLK-ASF1 pathway in inflammatory stress mediated AML progression. Mechanistically, our data show that ASF1B is regulated by IL-1β in a p38MAPK dependent manner (**Fig 2.5**). We observed that the transcription factors

MYBL2 and E2F1 were upregulated upon IL-1β stimulation, suggesting that they might be responsible for transcriptional upregulation of ASF1B. IL-1β did not transcriptionally upregulate TLK2, although its protein levels were increased. TLK2 protein levels are regulated by CRY2 (Correia et al., 2019), an E3-ubiquitin ligase that functions in the circadian cycle and MYBL2 was previously identified as a proximal interactor of TLK2, although the functional relevance of this interaction remains unclear (Pavinato et al., 2022). Therefore, the IL-1β pathway may have additional indirect effects on both TLK2 and ASF1B that remain to be discovered.

We observed that ASF1B or TLK2 deletion is dispensable for normal hematopoiesis (**Fig 2.11 and Fig 3.3**). Different from recent work on the roles of CHAF1B and HIRA in normal hematopoiesis. CHAF1B is part of CAF-1 interacts with ASF1 for chromatin assembly (Dong et al., 2001). Mx1-Cre/Chaf1b$^{f/f}$ mice died with pancytopenia within 2 weeks following plpC induced deletion and Vav-Cre+Chaf1b$^{f/f}$ pups were never observed. Chaf1b heterozygous mice exhibited modest reduction of bone marrow cells compared to wild-types. These results suggested that one allele of Chaf1b is sufficient for normal hematopoiesis (Volk et al., 2018). However, CHAF1B loss results in depletion of HSPCs in CHAF1B$^{-/-}$ mice and decrease LSK in CHAF1B$^{+/-}$ mice. HIRA is essential in mice and total knockout of HIRA leads to early embryonic death. Knockout of HIRA using Vav-Cre+ cause anemia, thrombocytopenia, and lymphocytopenia. Interestingly, HIRA-KO mice demonstrated reduction in B cell and T cell deficiency. HIRA deletion caused reduction in LKS in BM and impeded their progression to progenitors. (Chen et al., 2020). These results suggest that targeting TLK2 or ASF1B might an effective strategy to target leukemic cells while sparing healthy cells.

Together, we showed that chronic inflammation alters the intrinsic transcriptional landscape of AML and healthy progenitors, which further drives disease progression. Through the modulation of the TLK-ASF1 pathway, we demonstrated that it prevents inflammatory stress-mediated AML progression without affecting healthy cells.

Future direction 1: Targeting of TLK-ASF1 pathway

Our data show that targeting the TLK-ASF1 pathway reduced leukemia burden and progression *in vivo*, thus targeting this pathway represents a novel strategy for AML treatment. Previous work demonstrated the feasibility of targeting ASF1 binding to histones using a peptide inhibitor that binds to the histone binding pocket and reduced tumor size *in vivo* (Bakail et al., 2019). Several non-specific small-molecule inhibitors targeting TLK1 and TLK2 were tested in breast cancer (Kim et al., 2016) (Mortuza et al., 2018). Recent work reported improved versions of phenothiazine and bisindole derivatives that appear to have more potent effects on TLK1 and TLK2 inhibition (Lee et al., 2022; Singh et al., 2020), although their specificity and overall suitability for *in vivo* use remain unclear. Improved structure guided studies will be needed to optimize TLK inhibitors and future work is required to assess whether they will improve treatment efficacy alone or in combination with common AML targeted therapies. In the future, it will be interesting to test whether targeting ASF1 or TLK in combination with standard-of-care therapy will result in better patient outcomes in AML.

Future direction 2: Role of ASF1A and TLK1 *in vivo*

We have shown that deletion of ASF1B and TLK2 prolonged survival in an MLL-ENL AML model. However, ASF1B knockout mice and some of TLK2 mice eventually succumbed to the disease. It is possible that IL-1β upregulated other proteins or ASF1A compensated for ASF1B. We generated *Vav-Cre*$^{+}$*Asf1a*$^{F/F}$, *Vav-Cre*$^{+}$*Asf1a*$^{F/+}$, *Vav-Cre*$^{+}$*Asf1a*$^{F/+}$*Asf1b*$^{-/-}$, *Vav-Cre*$^{+}$*Asf1a*$^{F/F}$ *Asf1b*$^{+/-}$ mice. In the future, additional bone marrow transplantation studies will provide insight as to whether knockdown of both ASF1s will further extend survival as compared to ASF1A or ASF1B alone. We will also assess whether ASF1A deletion alone or deletion of both ASF1s affects normal hematopoiesis. We also generated *Vav-Cre*$^{+}$*Tlk1*$^{F/F}$, *Vav-Cre*$^{+}$*Tlk1*$^{F/+}$, *Vav-Cre*$^{+}$*Tlk1*$^{F/+}$*Tlk2*$^{-/-}$, *Vav-Cre*$^{+}$*Tlk1*$^{F/F}$*Tlk2*$^{+/-}$ mice and additional studies using these mice will identify the role of both TLKs in hematopoiesis *in vivo*.

Chapter 5: Materials and Methods

5.1 Primary samples

Peripheral blood or bone marrow of primary AML samples were obtained from patients evaluated at Oregon Health & Science University, University of Utah, University of Texas Southwestern Medical Center, University of Colorado, and Stanford University. All samples represented unique patients with AML and the clinical, genetic, and demographic information of AML patient samples is summarized in Table S1. Bone marrow mononuclear cells (MNCs) and purified CD34+ cells from normal donors were purchased commercially (Lonza Inc). MNCs from AML patient samples were isolated by Ficoll gradient centrifugation and red blood cells were lysed using an aqueous solution of 0.15 M NH_4Cl, 10 mM $KHCO_3$, and 0.1 mM EDTA. CD34+ cells were enriched using an immunomagnetic column (Miltenyi Biotech, San Diego, CA) and purity was evaluated using FACSAria IIIu flow cytometer (BD Biosciences, San Jose, CA). Primary cells were were cultured for the indicated time in cytokine-free media with IMDM supplemented with 10^{-4} M β-mercaptoethanol and 20% BIT (bovine insulin transferrin, Stem Cells Technologies). Studies using human cells were approved by the institutional review boards (IRBs).

5.2 Cell lines

All cell lines were tested negative for mycoplasma using MycoAlert mycoplasma detection kit (Lonza). 293T17 cells were used for retrovirus generation. 293T17 cells were cultured in Dulbecco's modified Eagle medium (DMEM, Gibco) supplemented with 10% FBS and 1% Pen/Strep. AML cell lines MOLM-14 and THP-1 (sourced from ATCC) were cultured

in RPMI-1640 (Gibco) supplemented with 2 mM L-glutamine, 1% Pen/Strep and 10% and 15% FBS, respectively. All cell lines were cultured at 37°C in 5% CO_2.

5.3 shRNA and Generation of lentivirus

Two independent and inducible small hairpin RNA (shRNA) libraries targeting TLK1, TLK2, ASF1A, ASF1B and two non-specific controls (NT16, NT17) were obtained from Cellecta Inc. shRNA #1 targets coding regions and shRNA #2 targets 3'UTR regions, respectively. Lentivirus was generated by transfecting 293FT cells using VSV-G envelope plasmid, psPAX2 helper plasmid, and FuGENE-6 reagent. Lentivirus particles were concentrated by ultracentrifuging the viral supernatant at 28,000 rpm for 2 h. MOLM-14 cells were infected with concentrated lentivirus in the presence of 5 μg/mL polybrene and 1 mM HEPES and centrifuged at 2,500 rpm for 90 min.

To obtain stable shRNA expression, this process was repeated at 48h and cells were GFP-, RFP- or GFP/RFP-sorted after 48 h of infection and maintained in 0.5 μg/mL puromycin. To induce shRNA expression, cells were treated with 1 μg/mL doxycycline and the effect of gene knockdown was assessed by immunoblotting, MTS cell viability, cell growth, cell cycle, and colony formation assays.

5.4 Cell viability, cell growth, cell cycle, and colony formation assays

For cell viability assay, 5 replicates of MOLM-14 cells (1200 cells/well) were plated in 384-well plates. After 3 or 6 days of culture, MTS reagent (CellTiter96 Aqueous One; Promega) was added and the optical density was measured at 490 nm. Raw absorbance values were adjusted to a reference blank value, normalized to untreated controls and presented as fold difference to determine cell viability. For cell growth assay, MOLM-14 cells were

plated at 0.2 e6 cells/well and kept at 0.5-1 e6/ml in triplicate. Cell count were measured by Guava easyCyte cell counter (Luminex) every other day. For cell cycle assay, MOLM-14 cells were fixed in cold 70% ethanol for 30 min on ice, washed with PBS, and treated with RNase. Cells were incubated with Propidium Iodide (50 μg/ml) for 30 min and analyzed using a FACSAria III flow cytometer (BD Bioscience). For colony formation assays, MOLM-14 cells (500 cells/well) were plated in triplicate in cytokine-free MethoCult H4230 (Stem Cell Technologies) and colonies were scored on Day 14.

5.5 Xenograft studies

MOLM-14 cells expressing doxycycline-inducible shASF1A, shASF1B, and shASF1A+B (2×10^5 cells per mouse) were injected into the tail veins of 4-week-old NOD-*scid* IL2Rg^{null} (NSG) mice purchased from Jackson Laboratories. After confirmation of equal engraftment in peripheral blood (>1%) by flow cytometry 5 days post injection, doxycycline chow (625 mg/kg; Envigo) was given to the mice to induce knockdown *in vivo*. Mice were monitored by complete blood counts using Heska Vet ABC blood analyzer (Scil Animal Care Company) and by GFP+, RFP+ or GFP/RFP+ percentage in peripheral blood using flow cytometry. For disease burden analysis, animals were sacrificed on day 18 post treatment, and weights of spleen and liver were measured. Cells from spleen, bone marrow, and peripheral blood were stained for fixable aqua dye, incubated at 37°C for 30 min, and stained for human cell surface markers: CD13 (PE-Cy7), CD33 (PE-Cy7), and CD15 (V450) as well as mouse pan hematopoietic cell surface marker CD45 (APC-Cy7) for 1 hour incubation at room temperature. The expressions of cell surface markers were measured by flow cytometry and analyzed using FlowJo software

5.6 Mice

All animal studies were approved by the Institutional Animal Care and Use Committee at OHSU (TR03_IP00000047) and conducted in accordance with the NIH guidelines for animal welfare. Animals were housed at semi-conventional facility and cared for according to standard guidelines at OHSU. Asf1bem1(IMPC)J, *Vav-iCre* and C57BL/6 mice were purchased from Jackson Laboratory. *Tlk2*$^{F/F}$ mice were generously provided by Dr. Travis Stracker (IRB Barcelona) (Segura-Bayona et al., 2017). *Tlk2*$^{F/F}$ mice were crossed with *Vav-iCre* mice in order to generate *Vav-Cre*$^{+}$*Tlk2*$^{F/+}$ and *Vav-Cre*$^{+}$*Tlk2*$^{F/F}$ hematopoietic specific conditional knockout mice. For genotyping, tail-tips were collected at weaning and analyzed by quantitative real time PCR (Transnetyx).

5.7 Generation of retrovirus

MLL-ENL-GFP retrovirus were generated by transfecting 293T17 cells with 5 μg of pEco-Pac helper plasmid and 30 μg of MLL-ENL-GFP vector (gifted by Dr. Scott Lowe, Dana Farber Cancer Institute) (Zuber et al., 2009) using Fugene 6 (Roche) as described previously (Agarwal et al., 2014). The virus particles were collected 48-72 hours post transfection. Human ASF1B was cloned into the pMSCV-IRES-mCherry FP vector using Gateway system (Invitrogen). ASF1B-mCherry and Empty-mCherry retrovirus were generated as described above.

5.8 Bone marrow transplantation and treatment

Bone marrow cells were isolated from femurs, tibias, and hipbones of 6 to 8-week-old *Asf1b*$^{+/+}$, *Asf1b*$^{+/-}$, *Asf1b*$^{-/-}$, *Vav-Cre*$^{-}$*Tlk2*$^{F/F}$, *Vav-Cre*$^{+}$*Tlk2*$^{F/+}$, and *Vav-Cre*$^{+}$*Tlk2*$^{F/F}$ donor

mice. Lineage negative cells were enriched using a Direct Lineage Cell Depletion Kit (Miltenyi Biotech) and pre-stimulated at 37°C overnight in DMEM supplemented with 1% Pen/Strep, 1X L-glutamine, 15% FBS, 15% WEHI-3B, 7 ng/mL murine IL-3, 12 ng/mL IL-6, and 56 ng/mL SCF. For ASF1B overexpression bone marrow transplantation, Lin- cells were infected with Empty-mCherry or ASF1B-mCherry retrovirus together with MLL-ENL-GFP retrovirus on fibronectin-coated plates through spinoculation (2 x 90 min, 2.500 rpm, 32ºC). 48 hours post-transduction, Lin-GFP+/RFP+ cells were sorted using a FACS Aria III flow cytometer (BD Biosciences). Sorted Lin-GFP+/RFP+ cells and supporting cells were retro-orbitally injected into lethally irradiated (500 + 450 cGy) 6-week old C57BL/6J recipient mice. For ASF1B and TLK2 deletion bone marrow transplantation, Lin- cells were infected with MLL-ENL-GFP retrovirus and Lin-GFP+ cells were sorted for injections. Mice were put on a soft food diet and antibiotic water for 2 weeks and were carefully monitored daily for signs of disease. Disease progression was monitored weekly by complete blood count using Heska Vet ABC blood analyzer (Scil Animal Care Company) and by GFP+/RFP+ or GFP+ percentage using FACS Aria III or CytoFlex S flow cytometer (BD Bioscience). Mouse IL-1 or vehicle was administered daily at 250 ng/mouse via intraperitoneal injection starting 14 days post-bone marrow transplant and throughout the studies. Morbid mice or mice that lost 20% weight were euthanized for further analysis. Bone marrow and spleen cells were stained with CD11b-APC, CD19-APC eFlour780, CD3-PE-Cy7, CD45-PE, Ter119-eFlour450, Ly6g/Ly6c-BV605, CD34-Alexa 700, cKit-APC-eFlour 780, Sca1-Pac Blue BV605-FcGamma and FVS510-viability.

5.9 Immunophenotyping of mouse cells

Peripheral blood was collected from *Asf1b*$^{+/+}$, *Asf1b*$^{+/-}$, *Asf1b*$^{-/-}$, *Vav-Cre*$^{-}$*Tlk2*$^{F/+}$ and *Vav-Cre*$^{+}$*Tlk2*$^{F/F}$ mice and analyzed by complete blood count. Bone marrow and spleen cells were immunophenotyped using APC-conjugated CD3, CD4, CD8, B220, Gr-1, Ter-119, CD19, IgM, and CD127 for lineage positive cells. Stem and progenitor cell populations were analyzed using fluorochrome-conjugated antibodies against mouse CD135-PercP-eFluor710, Sca-1-Pacific Blue, FCγ-BV605, CD48-BV711, CD150-PE-Cy7, CD34-Alexa700, and c-Kit-APC-eFluor780, and FVS510-viability dye. Both panels were analyzed using a LSRFortessa flow cytometer (BD Bioscience) to assess differentiation status. Various sub-populations are defined as follows: LKS (Lin-cKit+Sca-1+), LT-HSC (Lin-cKit+Sca-1+CD135-CD150+CD48-), ST-HSC (Lin-cKit+Sca-1+CD135-CD150-CD48-), multipotent progenitors including MPP2 (Lin-cKit+Sca-1+CD135-CD150+CD48+), MPP3 (Lin-cKit+Sca-1+CD135-CD150-CD48+), and MPP4 (Lin-cKit+Sca-1+CD135-CD150-). LK (Lin-cKit+Sca-1+) including common myeloid progenitor (CMP; Lin-cKit+Sca-1+ FCγ-CD34+), granulocyte/monocyte progenitor (GMP; Lin-cKit+Sca-1+ FCγ+CD34+), megakaryocyte/erythrocyte progenitor (MEP; Lin-cKit+Sca-1+ FCγ-CD34-).

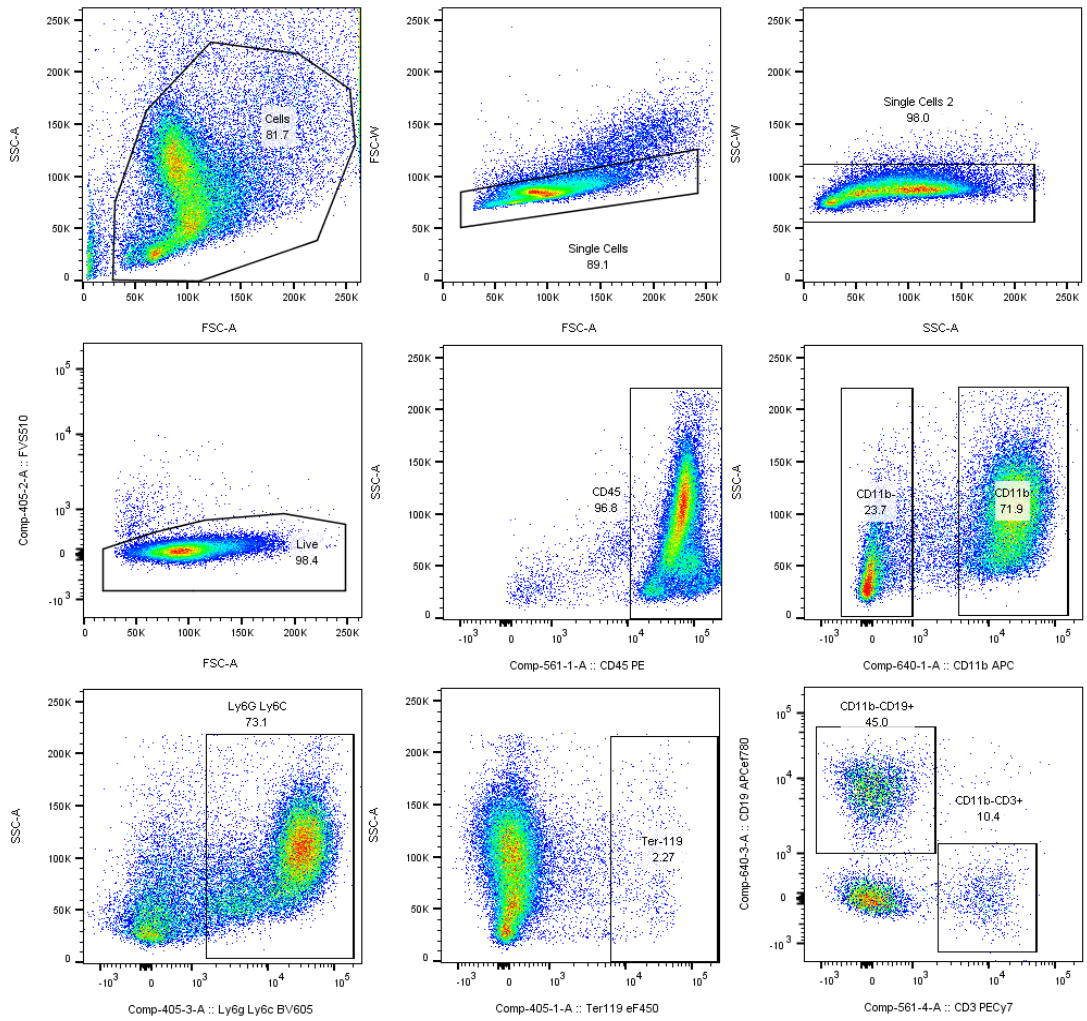

Figure 4.1 Gating strategies for immunophenotyping (myeloid and lymphoid cells)

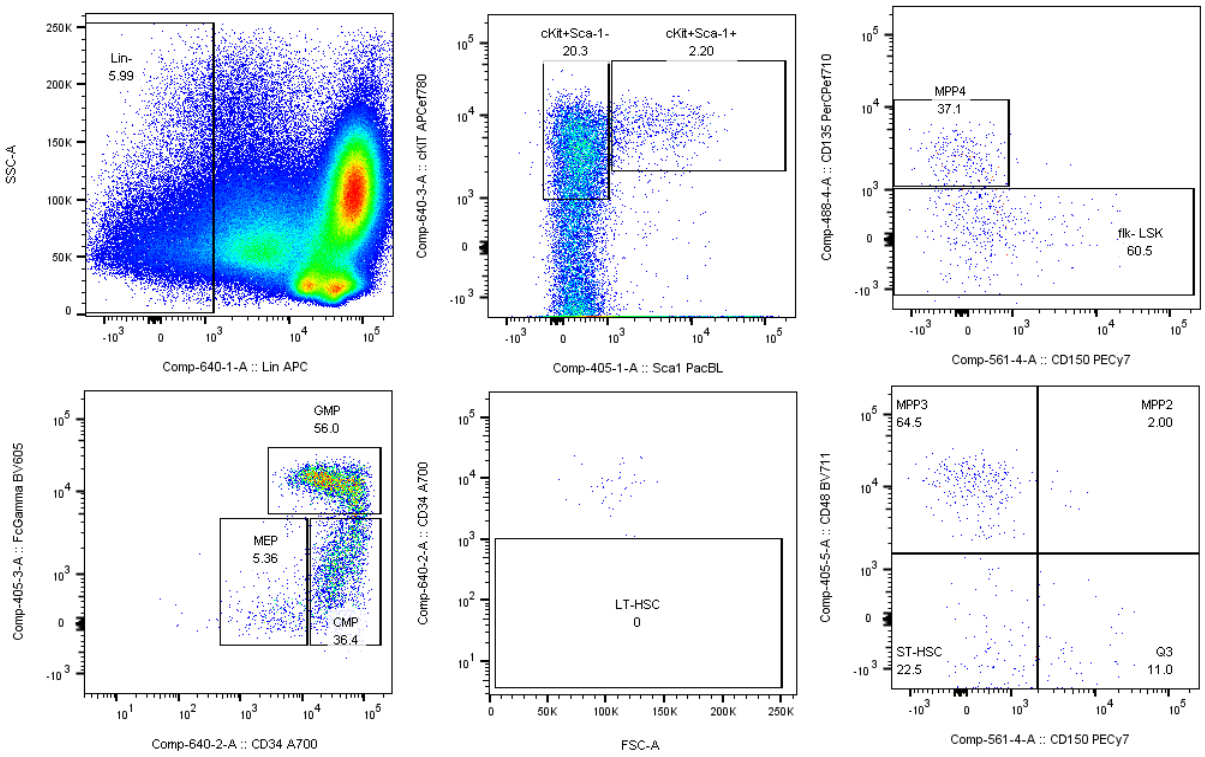

Figure 4.2 Gating strategies for immunophenotyping (stem and progenitor cells)

5.10 *In vivo* homing assay

Freshly harvested Lin- cells were stained with 100 nM carboxyfluorescein succinimidyl ester (CFSE) for 15 min at 37ºC. Further uptake of the dye was stopped by addition of an equal volume of sterile ice-cold FBS. Staining efficiency was confirmed by flow cytometry (LSRFortessa; BD Bioscience). 0.5×10^6 CFSE+ cells were retro-orbitally injected into 6-week old C57BL/6 WT mice. Mice were put on a soft food diet and antibiotic water and sacked 16 hours post-transplant. The percent of transplanted CFSE+ cells that homed to the bone marrow was calculated as follows: % Homing = (AxB/C)*100, where A is the percentage of CFSE+ cells determined by flow cytometry, B is the total organ cellularity, and C the number of cells transplanted (S.J. Szilvassy et al., 2001).

5.11 RNA-Seq analyses

mRNA was extracted from primary samples using RNeasy minikit following manufacturer's protocol. RNA-Seq libraries were generated using True-seq RNA exome kit (illumina) on a Sciclone platform (Perkin Elmer). mRNA underwent fragmentation, cDNA synthesis, and next-generation library synthesis via exome capture and PCR amplification. Libraries were sequenced on a Next-Seq instrument (illumina) using a paired-end protocol. Paired-end RNASeq samples (75 bp/read) were matched to the human (hg19) genomes and aligned with STAR. We used subread (Liao et al., 2019) to align to the human genome (hg19) and featureCounts (Liao et al., 2014) to quantify exon counts. We next summarized on a gene level by aggregating all exons per gene and summing the counts. We normalized the data using bioconductor's edgeR package (Robinson et al., 2010). We normalized using the Trimmed Mean of M Values (TMM)

method and calculated the Counts Per Million (CPM) for each gene. To identify samples that cluster together, we clustered based on CPM values.

5.12 Quantitative PCR

Primary cell pellets were stored at -80C. RNA extractions were performed using RNeasy mini kit (Qiagen) per manufacturer's instructions. RNA yield was quantified by nanodrop 1000 spectrophotometer. RNA was converted into cDNA using the High-Capacity cDNA Reverse Transcription Kit (Thermo Fisher Scientific). Quantitative PCR was performed using Platinum SYBR Green qPCR SuperMix (Thermo Fisher Scientific). PCR cycles were run using the QuantStudio 7 Flex System (Thermo Fisher Scientific) with standard cycle parameters.

5.13 TaqMan Gene Expression Array

A custom TaqMan low-density array (TLDA) was designed based on top hit candidate genes from RNA-Seq and biological relevance. RNA concentrations were measured with nanodrop and 150-2000 ng of RNA was reverse transcribed to complementary DNA using High-Capacity cDNA Reverse Transcription Kits (Applied Biosystems) and pre-amplified with a custom pool of primers and a PreAmp Master Mix. qPCR reactions were performed with the TaqMan Universal Master Mix II reagent in Custom TaqMan Array Cards (384-well plate preloaded with 96 specific primers of interest) on a PCR System. TLDA quantification was performed based on the manufacturer's protocol. All cards were run on the 12K Flex Real-Time PCR System (Applied Biosystems). Four treatment conditions for each sample were loaded on one card. The gene expression levels were determined and relatively quantified by using the comparative cycle threshold (Ct) method. Each plate

was adjusted by a normalization factor as the difference between the global median Ct value and the plate median Ct value. We calculated the expression of mRNAs with deltaCt, in which the maximal Ct value for an mRNA was subtracted from the specific value for this mRNA. The average of the replicate expression values of the mRNAs was used in the analysis. Each TLDA card has built-in controls including 18S, GUSB, and GAPDH. Genes and Assay IDs are provided in Table S4.

5.14 Western blot analysis

Whole-cell extracts were prepared by lysing cells for 20 min on ice in lysis buffer (Cell Signaling Technology) supplemented with a complete mini protease inhibitor cocktail tablet (Roche), phosphatase inhibitor (Sigma-Aldrich), and PMSF. Protein concentrations were quantified and normalized by a BCA assay (ThermoFisher Scientific). Lysates were separated through SDS polyacrylamide gels (4-12%) and transferred to nitrocellulose membrane (Bio-Rad). Membranes were blocked with 5% BSA in 0.1% Tween20 in 1x PBS (PBS-T) for 1 hr at room temperature followed by incubation with primary antibodies diluted in 5% BSA in PBST overnight at 4°C. The membrane was washed 3x in TBST before incubation with appropriate HRP-conjugated secondary antibodies for 1 h. Protein levels were visualized using ECL substrate (Bio-Rad) on a ChemiDoc MP Imaging System (Bio-Rad) with the Image Lab Software. Immunoblots were quantified using ImageJ software.

5.15 Analysis of Depmap, BeatAML, and TCGA databases

The dependency data used in this study was derived from the 20Q2 dataset. Dependency of TLK1, TLK2, ASF1A, ASF1B, E2F1, and MYBL2 from 20 AML cell lines were analyzed.

Expression data of TLK1, TLK2, ASF1A and ASF1B in various cancer types from the Cancer Cell Line Encyclopedia (CCLE) were also used. These data are available online: http://depmap.org/portal/download/all/. Expression of E2F1 and MYBL2 in ASF1B high (top 25%) and low (bottom 25%) patients from the TCGA database were analyzed via cBioportal. Characteristics of AML primary samples were obtained from the BeatAML database (Tyner et al., 2018).

Reference

Abascal, F., Corpet, A., Gurard-Levin, Z. A., Juan, D., Ochsenbein, F., Rico, D., Valencia, A., and Almouzni, G. (2013). Subfunctionalization via adaptive evolution influenced by genomic context: the case of histone chaperones ASF1a and ASF1b. Mol Biol Evol *30*, 1853-1866.

Agarwal, A., Mackenzie, R. J., Besson, A., Jeng, S., Carey, A., LaTocha, D. H., Fleischman, A. G., Duquesnes, N., Eide, C. A., Vasudevan, K. B., *et al.* (2014). BCR-ABL1 promotes leukemia by converting p27 into a cytoplasmic oncoprotein. Blood *124*, 3260-3273.

Antar, A. I., Otrock, Z. K., Jabbour, E., Mohty, M., and Bazarbachi, A. (2020). FLT3 inhibitors in acute myeloid leukemia: ten frequently asked questions. Leukemia *34*, 682-696.

Arber, D. A., Orazi, A., Hasserjian, R., Thiele, J., Borowitz, M. J., Le Beau, M. M., Bloomfield, C. D., Cazzola, M., and Vardiman, J. W. (2016). The 2016 revision to the World Health Organization classification of myeloid neoplasms and acute leukemia. Blood *127*, 2391-2405.

Arranz, L., Arriero, M. D. M., and Villatoro, A. (2017). Interleukin-1beta as emerging therapeutic target in hematological malignancies and potentially in their complications. Blood Rev *31*, 306-317.

Awate, S., and De Benedetti, A. (2016). TLK1B mediated phosphorylation of Rad9 regulates its nuclear/cytoplasmic localization and cell cycle checkpoint. BMC Mol Biol *17*, 3.

Bakail, M., Gaubert, A., Andreani, J., Moal, G., Pinna, G., Boyarchuk, E., Gaillard, M. C., Courbeyrette, R., Mann, C., Thuret, J. Y., *et al.* (2019). Design on a Rational Basis of High-Affinity Peptides Inhibiting the Histone Chaperone ASF1. Cell Chem Biol *26*, 1573-1585 e1510.

Barretina, J., Caponigro, G., Stransky, N., Venkatesan, K., Margolin, A. A., Kim, S., Wilson, C. J., Lehar, J., Kryukov, G. V., Sonkin, D., *et al.* (2012). The Cancer Cell Line Encyclopedia enables predictive modelling of anticancer drug sensitivity. Nature *483*, 603-607.

Barreyro, L., Will, B., Bartholdy, B., Zhou, L., Todorova, T. I., Stanley, R. F., Ben-Neriah, S., Montagna, C., Parekh, S., Pellagatti, A., *et al.* (2012). Overexpression of IL-1 receptor accessory protein in stem and progenitor cells and outcome correlation in AML and MDS. Blood *120*, 1290-1298.

Battu, A., Ray, A., and Wani, A. A. (2011). ASF1A and ATM regulate H3K56-mediated cell-cycle checkpoint recovery in response to UV irradiation. Nucleic Acids Res *39*, 7931-7945.

Bennett, J. M., Catovsky, D., Daniel, M. T., Flandrin, G., Galton, D. A., Gralnick, H. R., and Sultan, C. (1976). Proposals for the classification of the acute leukaemias. French-American-British (FAB) co-operative group. Br J Haematol *33*, 451-458.

Binder, S., Luciano, M., and Horejs-Hoeck, J. (2018). The cytokine network in acute myeloid leukemia (AML): A focus on pro- and anti-inflammatory mediators. Cytokine Growth Factor Rev *43*, 8-15.

Bruinsma, W., van den Berg, J., Aprelia, M., and Medema, R. H. (2016). Tousled-like kinase 2 regulates recovery from a DNA damage-induced G2 arrest. EMBO Rep *17*, 659-670.

Caiado, F., Pietras, E. M., and Manz, M. G. (2021). Inflammation as a regulator of hematopoietic stem cell function in disease, aging, and clonal selection. J Exp Med *218*.

Cancer Genome Atlas Research, N., Ley, T. J., Miller, C., Ding, L., Raphael, B. J., Mungall, A. J., Robertson, A., Hoadley, K., Triche, T. J., Jr., Laird, P. W., *et al.* (2013). Genomic and epigenomic landscapes of adult de novo acute myeloid leukemia. N Engl J Med *368*, 2059-2074.

Carey, A., Edwards, D. K. t., Eide, C. A., Newell, L., Traer, E., Medeiros, B. C., Pollyea, D. A., Deininger, M. W., Collins, R. H., Tyner, J. W., *et al.* (2017). Identification of Interleukin-1 by Functional Screening as a Key Mediator of Cellular Expansion and Disease Progression in Acute Myeloid Leukemia. Cell Rep *18*, 3204-3218.

Carter, B. Z., Mak, P. Y., Wang, X., Tao, W., Ruvolo, V., Mak, D., Mu, H., Burks, J. K., and Andreeff, M. (2019). An ARC-Regulated IL1beta/Cox-2/PGE2/beta-Catenin/ARC Circuit Controls Leukemia-Microenvironment Interactions and Confers Drug Resistance in AML. Cancer Res *79*, 1165-1177.

Chen, C., Sun, M. A., Warzecha, C., Bachu, M., Dey, A., Wu, T., Adams, P. D., Macfarlan, T., Love, P., and Ozato, K. (2020). HIRA, a DiGeorge Syndrome Candidate Gene, Confers Proper Chromatin Accessibility on HSCs and Supports All Stages of Hematopoiesis. Cell Rep *30*, 2136-2149 e2134.

Corpet, A., De Koning, L., Toedling, J., Savignoni, A., Berger, F., Lemaitre, C., O'Sullivan, R. J., Karlseder, J., Barillot, E., Asselain, B., *et al.* (2011). Asf1b, the necessary Asf1 isoform for proliferation, is predictive of outcome in breast cancer. EMBO J *30*, 480-493.

Correia, S. P., Chan, A. B., Vaughan, M., Zolboot, N., Perea, V., Huber, A. L., Kriebs, A., Moresco, J. J., Yates, J. R., 3rd, and Lamia, K. A. (2019). The circadian E3 ligase complex SCF(FBXL3+CRY) targets TLK2. Sci Rep *9*, 198.

Das, C., Lucia, M. S., Hansen, K. C., and Tyler, J. K. (2009). CBP/p300-mediated acetylation of histone H3 on lysine 56. Nature *459*, 113-117.

De Boer, B., Sheveleva, S., Apelt, K., Vellenga, E., Mulder, A. B., Huls, G., and Jacob Schuringa, J. (2021). The IL1-IL1RAP axis plays an important role in the inflammatory leukemic niche that favors acute myeloid leukemia proliferation over normal hematopoiesis. Haematologica *106*, 3067-3078.

Delacote, F., and Lopez, B. S. (2008). Importance of the cell cycle phase for the choice of the appropriate DSB repair pathway, for genome stability maintenance: the trans-S double-strand break repair model. Cell Cycle *7*, 33-38.

DiNardo, C. D., Pratz, K. W., Letai, A., Jonas, B. A., Wei, A. H., Thirman, M., Arellano, M., Frattini, M. G., Kantarjian, H., Popovic, R., *et al.* (2018). Safety and preliminary efficacy of venetoclax with decitabine or azacitidine in elderly patients with previously untreated acute myeloid leukaemia: a non-randomised, open-label, phase 1b study. Lancet Oncol *19*, 216-228.

Dinarello, C. A., Simon, A., and van der Meer, J. W. (2012). Treating inflammation by blocking interleukin-1 in a broad spectrum of diseases. Nat Rev Drug Discov *11*, 633-652.

Dohner, H., Weisdorf, D. J., and Bloomfield, C. D. (2015). Acute Myeloid Leukemia. N Engl J Med *373*, 1136-1152.

Dong, H., Lin, W., Zhang, C. K., Xiong, H., Fu, G., Jin, W. R., Chen, R., Chen, Z., Qi, Z. T., and Huang, G. M. (2001). Genomic sequence and expression analyses of human chromatin assembly factor 1 p150 gene. Gene *264*, 187-196.

English, C. M., Adkins, M. W., Carson, J. J., Churchill, M. E., and Tyler, J. K. (2006). Structural basis for the histone chaperone activity of Asf1. Cell *127*, 495-508.

Estey, E., and Dohner, H. (2006). Acute myeloid leukaemia. Lancet *368*, 1894-1907.
Fang, J., Bolanos, L. C., Choi, K., Liu, X., Christie, S., Akunuru, S., Kumar, R., Wang, D., Chen, X., Greis, K. D., *et al.* (2017). Ubiquitination of hnRNPA1 by TRAF6 links chronic innate immune signaling with myelodysplasia. Nat Immunol *18*, 236-245.

Feng, S., Ma, S., Li, K., Gao, S., Ning, S., Shang, J., Guo, R., Chen, Y., Blumenfeld, B., Simon, I., *et al.* (2022). RIF1-ASF1-mediated high-order chromatin structure safeguards genome integrity. Nat Commun *13*, 957.

Gao, J., Aksoy, B. A., Dogrusoz, U., Dresdner, G., Gross, B., Sumer, S. O., Sun, Y., Jacobsen, A., Sinha, R., Larsson, E., *et al.* (2013). Integrative analysis of complex cancer genomics and clinical profiles using the cBioPortal. Sci Signal *6*, pl1.

Gomes, A. P., Ilter, D., Low, V., Rosenzweig, A., Shen, Z. J., Schild, T., Rivas, M. A., Er, E. E., McNally, D. R., Mutvei, A. P., *et al.* (2019). Dynamic Incorporation of Histone H3 Variants into Chromatin Is Essential for Acquisition of Aggressive Traits and Metastatic Colonization. Cancer Cell *36*, 402-417 e413.

Gram, H. (2016). Preclinical characterization and clinical development of ILARIS((R)) (canakinumab) for the treatment of autoinflammatory diseases. Curr Opin Chem Biol *32*, 1-9.

Groschel, S., Sanders, M. A., Hoogenboezem, R., Zeilemaker, A., Havermans, M., Erpelinck, C., Bindels, E. M., Beverloo, H. B., Dohner, H., Lowenberg, B., *et al.* (2015). Mutational spectrum

of myeloid malignancies with inv(3)/t(3;3) reveals a predominant involvement of RAS/RTK signaling pathways. Blood *125*, 133-139.

Groth, A., Corpet, A., Cook, A. J., Roche, D., Bartek, J., Lukas, J., and Almouzni, G. (2007). Regulation of replication fork progression through histone supply and demand. Science *318*, 1928-1931.

Groth, A., Lukas, J., Nigg, E. A., Sillje, H. H., Wernstedt, C., Bartek, J., and Hansen, K. (2003). Human Tousled like kinases are targeted by an ATM- and Chk1-dependent DNA damage checkpoint. EMBO J *22*, 1676-1687.

Hayashi, R., Goto, Y., Tanaka, R., Oonogi, K., Hisasue, M., and Yoshida, K. (2007). Transcriptional regulation of human chromatin assembly factor ASF1. DNA Cell Biol *26*, 91-99.

Hernandez, G., Mills, T. S., Rabe, J. L., Chavez, J. S., Kuldanek, S., Kirkpatrick, G., Noetzli, L., Jubair, W. K., Zanche, M., Myers, J. R., *et al.* (2020). Pro-inflammatory cytokine blockade attenuates myeloid expansion in a murine model of rheumatoid arthritis. Haematologica *105*, 585-597.

Hosseini, M. M., Kurtz, S. E., Abdelhamed, S., Mahmood, S., Davare, M. A., Kaempf, A., Elferich, J., McDermott, J. E., Liu, T., Payne, S. H., *et al.* (2018). Inhibition of interleukin-1 receptor-associated kinase-1 is a therapeutic strategy for acute myeloid leukemia subtypes. Leukemia *32*, 2374-2387.

Huang, T. H., Fowler, F., Chen, C. C., Shen, Z. J., Sleckman, B., and Tyler, J. K. (2020). The Histone Chaperones ASF1 and CAF-1 Promote MMS22L-TONSL-Mediated Rad51 Loading onto ssDNA during Homologous Recombination in Human Cells. Mol Cell *77*, 1153.

Jaiswal, S., Fontanillas, P., Flannick, J., Manning, A., Grauman, P. V., Mar, B. G., Lindsley, R. C., Mermel, C. H., Burtt, N., Chavez, A., *et al.* (2014). Age-related clonal hematopoiesis associated with adverse outcomes. N Engl J Med *371*, 2488-2498.

Kelly, R., and Davey, S. K. (2013). Tousled-like kinase-dependent phosphorylation of Rad9 plays a role in cell cycle progression and G2/M checkpoint exit. PLoS One *8*, e85859.

Kim, J. A., Tan, Y., Wang, X., Cao, X., Veeraraghavan, J., Liang, Y., Edwards, D. P., Huang, S., Pan, X., Li, K., *et al.* (2016). Comprehensive functional analysis of the tousled-like kinase 2 frequently amplified in aggressive luminal breast cancers. Nat Commun *7*, 12991.

Klimovskaia, I. M., Young, C., Stromme, C. B., Menard, P., Jasencakova, Z., Mejlvang, J., Ask, K., Ploug, M., Nielsen, M. L., Jensen, O. N., and Groth, A. (2014). Tousled-like kinases phosphorylate Asf1 to promote histone supply during DNA replication. Nat Commun *5*, 3394.

Konopleva, M., Pollyea, D. A., Potluri, J., Chyla, B., Hogdal, L., Busman, T., McKeegan, E., Salem, A. H., Zhu, M., Ricker, J. L., *et al.* (2016). Efficacy and Biological Correlates of

Response in a Phase II Study of Venetoclax Monotherapy in Patients with Acute Myelogenous Leukemia. Cancer Discov *6*, 1106-1117.

Kornberg, R. D. (1974). Chromatin structure: a repeating unit of histones and DNA. Science *184*, 868-871.

Kristinsson, S. Y., Bjorkholm, M., Hultcrantz, M., Derolf, A. R., Landgren, O., and Goldin, L. R. (2011). Chronic immune stimulation might act as a trigger for the development of acute myeloid leukemia or myelodysplastic syndromes. J Clin Oncol *29*, 2897-2903.

Lee, K. Y., and Dutta, A. (2021). Chk1 promotes non-homologous end joining in G1 through direct phosphorylation of ASF1A. Cell Rep *34*, 108680.

Lee, K. Y., Im, J. S., Shibata, E., and Dutta, A. (2017). ASF1a Promotes Non-homologous End Joining Repair by Facilitating Phosphorylation of MDC1 by ATM at Double-Strand Breaks. Mol Cell *68*, 61-75 e65.

Lee, S. B., Chang, T. Y., Lee, N. Z., Yu, Z. Y., Liu, C. Y., and Lee, H. Y. (2022). Design, synthesis and biological evaluation of bisindole derivatives as anticancer agents against Tousled-like kinases. Eur J Med Chem *227*, 113904.

Lee, S. B., Segura-Bayona, S., Villamor-Paya, M., Saredi, G., Todd, M. A. M., Attolini, C. S., Chang, T. Y., Stracker, T. H., and Groth, A. (2018). Tousled-like kinases stabilize replication forks and show synthetic lethality with checkpoint and PARP inhibitors. Sci Adv *4*, eaat4985.

Letai, A. G. (2008). Diagnosing and exploiting cancer's addiction to blocks in apoptosis. Nat Rev Cancer *8*, 121-132.

Li, F., Huang, Q., Luster, T. A., Hu, H., Zhang, H., Ng, W. L., Khodadadi-Jamayran, A., Wang, W., Chen, T., Deng, J., *et al.* (2020). In Vivo Epigenetic CRISPR Screen Identifies Asf1a as an Immunotherapeutic Target in Kras-Mutant Lung Adenocarcinoma. Cancer Discov *10*, 270-287.

Li, J., Volk, A., Zhang, J., Cannova, J., Dai, S., Hao, C., Hu, C., Sun, J., Xu, Y., Wei, W., *et al.* (2017). Sensitizing leukemia stem cells to NF-kappaB inhibitor treatment in vivo by inactivation of both TNF and IL-1 signaling. Oncotarget *8*, 8420-8435.

Li, S., Mason, C. E., and Melnick, A. (2016). Genetic and epigenetic heterogeneity in acute myeloid leukemia. Curr Opin Genet Dev *36*, 100-106.

Liang, K., Volk, A. G., Haug, J. S., Marshall, S. A., Woodfin, A. R., Bartom, E. T., Gilmore, J. M., Florens, L., Washburn, M. P., Sullivan, K. D., *et al.* (2017). Therapeutic Targeting of MLL Degradation Pathways in MLL-Rearranged Leukemia. Cell *168*, 59-72 e13.

Liao, Y., Smyth, G. K., and Shi, W. (2014). featureCounts: an efficient general purpose program for assigning sequence reads to genomic features. Bioinformatics *30*, 923-930.

Liao, Y., Smyth, G. K., and Shi, W. (2019). The R package Rsubread is easier, faster, cheaper and better for alignment and quantification of RNA sequencing reads. Nucleic Acids Res *47*, e47.

Liu, X., Song, J., Zhang, Y., Wang, H., Sun, H., Feng, X., Hou, M., Chen, G., Tang, Q., and Ji, M. (2020). ASF1B promotes cervical cancer progression through stabilization of CDK9. Cell Death Dis *11*, 705.

Ma, J., Han, W., and Lu, K. (2021). Comprehensive Pan-Cancer Analysis and the Regulatory Mechanism of ASF1B, a Gene Associated With Thyroid Cancer Prognosis in the Tumor Micro-Environment. Front Oncol *11*, 711756.

Martire, S., and Banaszynski, L. A. (2020). The roles of histone variants in fine-tuning chromatin organization and function. Nat Rev Mol Cell Biol *21*, 522-541.

McMahon, C. M., Ferng, T., Canaani, J., Wang, E. S., Morrissette, J. J. D., Eastburn, D. J., Pellegrino, M., Durruthy-Durruthy, R., Watt, C. D., Asthana, S., *et al.* (2019). Clonal Selection with RAS Pathway Activation Mediates Secondary Clinical Resistance to Selective FLT3 Inhibition in Acute Myeloid Leukemia. Cancer Discov *9*, 1050-1063.

McMurry, H., Fletcher, L., and Traer, E. (2021). IDH Inhibitors in AML-Promise and Pitfalls. Curr Hematol Malig Rep *16*, 207-217.

Mortuza, G. B., Hermida, D., Pedersen, A. K., Segura-Bayona, S., Lopez-Mendez, B., Redondo, P., Ruther, P., Pozdnyakova, I., Garrote, A. M., Munoz, I. G., *et al.* (2018). Molecular basis of Tousled-Like Kinase 2 activation. Nat Commun *9*, 2535.

Nechiporuk, T., Kurtz, S. E., Nikolova, O., Liu, T., Jones, C. L., D'Alessandro, A., Culp-Hill, R., d'Almeida, A., Joshi, S. K., Rosenberg, M., *et al.* (2019). The TP53 Apoptotic Network Is a Primary Mediator of Resistance to BCL2 Inhibition in AML Cells. Cancer Discov *9*, 910-925.

O'Sullivan, R. J., Arnoult, N., Lackner, D. H., Oganesian, L., Haggblom, C., Corpet, A., Almouzni, G., and Karlseder, J. (2014). Rapid induction of alternative lengthening of telomeres by depletion of the histone chaperone ASF1. Nat Struct Mol Biol *21*, 167-174.

Orkin, S. H., and Zon, L. I. (2008). Hematopoiesis: an evolving paradigm for stem cell biology. Cell *132*, 631-644.

Panier, S., and Boulton, S. J. (2014). Double-strand break repair: 53BP1 comes into focus. Nat Rev Mol Cell Biol *15*, 7-18.

Papaemmanuil, E., Dohner, H., and Campbell, P. J. (2016). Genomic Classification in Acute Myeloid Leukemia. N Engl J Med *375*, 900-901.

Park, Y. J., and Luger, K. (2008). Histone chaperones in nucleosome eviction and histone exchange. Curr Opin Struct Biol *18*, 282-289.

Pavinato, L., Villamor-Paya, M., Sanchiz-Calvo, M., Andreoli, C., Gay, M., Vilaseca, M., Arauz-Garofalo, G., Ciolfi, A., Bruselles, A., Pippucci, T., *et al.* (2022). Functional analysis of TLK2 variants and their proximal interactomes implicates impaired kinase activity and chromatin maintenance defects in their pathogenesis. J Med Genet *59*, 170-179.

Pietras, E. M. (2017). Inflammation: a key regulator of hematopoietic stem cell fate in health and disease. Blood *130*, 1693-1698.

Pietras, E. M., Mirantes-Barbeito, C., Fong, S., Loeffler, D., Kovtonyuk, L. V., Zhang, S., Lakshminarasimhan, R., Chin, C. P., Techner, J. M., Will, B., *et al.* (2016). Chronic interleukin-1 exposure drives haematopoietic stem cells towards precocious myeloid differentiation at the expense of self-renewal. Nat Cell Biol *18*, 607-618.

Pietras, E. M., Warr, M. R., and Passegue, E. (2011). Cell cycle regulation in hematopoietic stem cells. J Cell Biol *195*, 709-720.

Pilyugin, M., Demmers, J., Verrijzer, C. P., Karch, F., and Moshkin, Y. M. (2009). Phosphorylation-mediated control of histone chaperone ASF1 levels by Tousled-like kinases. PLoS One *4*, e8328.

Robinson, M. D., McCarthy, D. J., and Smyth, G. K. (2010). edgeR: a Bioconductor package for differential expression analysis of digital gene expression data. Bioinformatics *26*, 139-140.

Roe, J. L., Rivin, C. J., Sessions, R. A., Feldmann, K. A., and Zambryski, P. C. (1993). The Tousled gene in A. thaliana encodes a protein kinase homolog that is required for leaf and flower development. Cell *75*, 939-950.

Ronald, S., Awate, S., Rath, A., Carroll, J., Galiano, F., Dwyer, D., Kleiner-Hancock, H., Mathis, J. M., Vigod, S., and De Benedetti, A. (2013). Phenothiazine Inhibitors of TLKs Affect Double-Strand Break Repair and DNA Damage Response Recovery and Potentiate Tumor Killing with Radiomimetic Therapy. Genes Cancer *4*, 39-53.

Sabattini, E., Bacci, F., Sagramoso, C., and Pileri, S. A. (2010). WHO classification of tumours of haematopoietic and lymphoid tissues in 2008: an overview. Pathologica *102*, 83-87.

Sanchez-Correa, B., Bergua, J. M., Campos, C., Gayoso, I., Arcos, M. J., Banas, H., Morgado, S., Casado, J. G., Solana, R., and Tarazona, R. (2013). Cytokine profiles in acute myeloid leukemia patients at diagnosis: survival is inversely correlated with IL-6 and directly correlated with IL-10 levels. Cytokine *61*, 885-891.

Segura-Bayona, S., Knobel, P. A., Gonzalez-Buron, H., Youssef, S. A., Pena-Blanco, A., Coyaud, E., Lopez-Rovira, T., Rein, K., Palenzuela, L., Colombelli, J., *et al.* (2017). Differential requirements for Tousled-like kinases 1 and 2 in mammalian development. Cell Death Differ *24*, 1872-1885.

Segura-Bayona, S., and Stracker, T. H. (2019). The Tousled-like kinases regulate genome and epigenome stability: implications in development and disease. Cell Mol Life Sci *76*, 3827-3841.

Segura-Bayona, S., Villamor-Paya, M., Attolini, C. S., Koenig, L. M., Sanchiz-Calvo, M., Boulton, S. J., and Stracker, T. H. (2020). Tousled-Like Kinases Suppress Innate Immune Signaling Triggered by Alternative Lengthening of Telomeres. Cell Rep *32*, 107983.

Shlush, L. I., Zandi, S., Mitchell, A., Chen, W. C., Brandwein, J. M., Gupta, V., Kennedy, J. A., Schimmer, A. D., Schuh, A. C., Yee, K. W., *et al.* (2014). Identification of pre-leukaemic haematopoietic stem cells in acute leukaemia. Nature *506*, 328-333.

Sillje, H. H., Takahashi, K., Tanaka, K., Van Houwe, G., and Nigg, E. A. (1999). Mammalian homologues of the plant Tousled gene code for cell-cycle-regulated kinases with maximal activities linked to ongoing DNA replication. EMBO J *18*, 5691-5702.

Simon, B., Lou, H. J., Huet-Calderwood, C., Shi, G., Boggon, T. J., Turk, B. E., and Calderwood, D. A. (2022). Tousled-like kinase 2 targets ASF1 histone chaperones through client mimicry. Nat Commun *13*, 749.

Sims, J. E., and Smith, D. E. (2010). The IL-1 family: regulators of immunity. Nat Rev Immunol *10*, 89-102.

Singh, V., Bhoir, S., Chikhale, R. V., Hussain, J., Dwyer, D., Bryce, R. A., Kirubakaran, S., and De Benedetti, A. (2020). Generation of Phenothiazine with Potent Anti-TLK1 Activity for Prostate Cancer Therapy. iScience *23*, 101474.

Singh, V., Jaiswal, P. K., Ghosh, I., Koul, H. K., Yu, X., and De Benedetti, A. (2019a). Targeting the TLK1/NEK1 DDR axis with Thioridazine suppresses outgrowth of androgen independent prostate tumors. Int J Cancer *145*, 1055-1067.

Singh, V., Jaiswal, P. K., Ghosh, I., Koul, H. K., Yu, X., and De Benedetti, A. (2019b). The TLK1-Nek1 axis promotes prostate cancer progression. Cancer Lett *453*, 131-141.

Smith, M. A., Choudhary, G. S., Pellagatti, A., Choi, K., Bolanos, L. C., Bhagat, T. D., Gordon-Mitchell, S., Von Ahrens, D., Pradhan, K., Steeples, V., *et al.* (2019). U2AF1 mutations induce oncogenic IRAK4 isoforms and activate innate immune pathways in myeloid malignancies. Nat Cell Biol *21*, 640-650.

Szklarczyk, D., Gable, A. L., Nastou, K. C., Lyon, D., Kirsch, R., Pyysalo, S., Doncheva, N. T., Legeay, M., Fang, T., Bork, P., *et al.* (2021). The STRING database in 2021: customizable protein-protein networks, and functional characterization of user-uploaded gene/measurement sets. Nucleic Acids Res *49*, D605-D612.

Tang, M., Chen, Z., Wang, C., Feng, X., Lee, N., Huang, M., Zhang, H., Li, S., Xiong, Y., and Chen, J. (2022). Histone chaperone ASF1 acts with RIF1 to promote DNA end-joining in BRCA1-deficient cells. J Biol Chem, 101979.

Trowbridge, J. J., and Starczynowski, D. T. (2021). Innate immune pathways and inflammation in hematopoietic aging, clonal hematopoiesis, and MDS. J Exp Med *218*.

Tyner, J. W., Tognon, C. E., Bottomly, D., Wilmot, B., Kurtz, S. E., Savage, S. L., Long, N., Schultz, A. R., Traer, E., Abel, M., *et al.* (2018). Functional genomic landscape of acute myeloid leukaemia. Nature *562*, 526-531.

Volk, A., Li, J., Xin, J., You, D., Zhang, J., Liu, X., Xiao, Y., Breslin, P., Li, Z., Wei, W., *et al.* (2014). Co-inhibition of NF-kappaB and JNK is synergistic in TNF-expressing human AML. J Exp Med *211*, 1093-1108.

Volk, A., Liang, K., Suraneni, P., Li, X., Zhao, J., Bulic, M., Marshall, S., Pulakanti, K., Malinge, S., Taub, J., *et al.* (2018). A CHAF1B-Dependent Molecular Switch in Hematopoiesis and Leukemia Pathogenesis. Cancer Cell *34*, 707-723 e707.

Wilson, A., Laurenti, E., Oser, G., van der Wath, R. C., Blanco-Bose, W., Jaworski, M., Offner, S., Dunant, C. F., Eshkind, L., Bockamp, E., *et al.* (2008). Hematopoietic stem cells reversibly switch from dormancy to self-renewal during homeostasis and repair. Cell *135*, 1118-1129.
Wu, Y., Li, X., Yu, J., Bjorkholm, M., and Xu, D. (2019). ASF1a inhibition induces p53-dependent growth arrest and senescence of cancer cells. Cell Death Dis *10*, 76.

Xie, Y., Sahin, M., Sinha, S., Wang, Y., Nargund, A. M., Lyu, Y., Han, S., Dong, Y., Hsieh, J. J., Leslie, C. S., and Cheng, E. H. (2022). SETD2 loss perturbs the kidney cancer epigenetic landscape to promote metastasis and engenders actionable dependencies on histone chaperone complexes. Nat Cancer *3*, 188-202.

Yang, S., Liu, L., Cao, C., Song, N., Wang, Y., Ma, S., Zhang, Q., Yu, N., Ding, X., Yang, F., *et al.* (2018). USP52 acts as a deubiquitinase and promotes histone chaperone ASF1A stabilization. Nat Commun *9*, 1285.

Zhang, T. Y., Dutta, R., Benard, B., Zhao, F., Yin, R., and Majeti, R. (2020). IL-6 blockade reverses bone marrow failure induced by human acute myeloid leukemia. Sci Transl Med *12*.

Zuber, J., Radtke, I., Pardee, T. S., Zhao, Z., Rappaport, A. R., Luo, W., McCurrach, M. E., Yang, M. M., Dolan, M. E., Kogan, S. C., *et al.* (2009). Mouse models of human AML accurately predict chemotherapy response. Genes Dev *23*, 877-889.

Table 1. Genes for TLDA validation

ADAMTS14	Hs00365506_m1
APOL4	Hs00540930_m1
ARHGAP24	Hs01097578_m1
ASF1B	Hs00216780_m1
BIRC3	Hs00985031_g1
C1QB	Hs00608019_m1
CCDC170	Hs00228128_m1
CCL2	Hs00234140_m1
CCNA2	Hs00996788_m1
CD207	Hs00210453_m1
CD40	Hs01002913_g1
CDC6	Hs00154374_m1
CHAF1B	Hs01123297_m1
CLSPN	Hs00898637_m1
CSF2	Hs00929873_m1
E2F2	Hs00231667_m1
GGT5	Hs00269779_m1
GIMAP8	Hs00411000_m1
GNAO1	Hs00221365_m1
GNAZ	Hs00157731_m1
HBD	Hs00426283_m1
HIST1H1B	Hs00271207_s1
HIST1H2AJ	Hs04191486_s1
HTRA1	Hs01016151_m1
IL8	Hs00174103_m1
ICAM1	Hs00164932_m1
IKBKB	Hs00233287_m1
LCNL1	Hs01115021_m1
MAD2L1	Hs01554513_g1
MARCKS	Hs00158993_m1
MCM5	Hs01052148_m1
NMT1	Hs00221506_m1
NUF2	Hs00230097_m1
PIK3R1	Hs00933163_m1
RRM2	Hs00357247_g1
SIRT1	Hs01009006_m1
TNFRSF9	Hs00155512_m1

VCAN	Hs00171642_m1
IL1A	Hs00174092_m1
IL1B	Hs00174097_m1
IL1R1	Hs00991010_m1
IL1RAP	Hs00895050_m1
IRAK1	Hs00155570_m1
IRAK4	Hs00211610_m1
JUN	Hs01103582_s1
TLK1	Hs00895309_m1
TLK2	Hs00851784_g1

Table 2. AML patient characteristics

Sample ID	Gender	Age at Diagnosis	Specific Diagnosis	Specimen Type	Use
AML-1	Male	68	AML with myelodysplasia-related changes	Leukapheresis	WB
AML-2	Female	53	AML with maturation	Bone Marrow Aspirate	WB
AML-3	Female	63	AML with mutated NPM1	Peripheral Blood	WB
AML-4	Male	70	AML with mutated NPM1	Peripheral Blood	WB
AML-5	Female	61	AML with mutated NPM1	Peripheral Blood	WB
AML-6	Female	67	Therapy-related myeloid neoplasms	Peripheral Blood	WB
AML-7	Male	55	Acute myeloid leukaemia, NOS	Bone Marrow Aspirate	WB
AML-8	Male	50	Therapy-related myeloid neoplasms	Bone Marrow Aspirate	WB
AML-9	Male	80	Acute myeloid leukaemia, NOS	Bone Marrow Aspirate	RNA-Seq
AML-10	Male	75	Acute myeloid leukaemia, NOS	Bone Marrow Aspirate	RNA-Seq
AML-11	Male	61	Acute myeloid leukaemia, NOS	Bone Marrow Aspirate	RNA-Seq
AML-12	Male	44	AML with inv(16)(p13.1q22) or t(16;16)(p13.1;q22); CBFB-MYH11	Peripheral Blood	TLDA
AML-13	Male	66	Acute monoblastic and monocytic leukaemia	Leukapheresis	TLDA
AML-14	Male	51	Unknown	Bone Marrow Aspirate	TLDA
AML-15	Male	61	AML with minimal differentiation	Bone Marrow Aspirate	TLDA

Table 3. Reagents and resources

Antibodies		
Rabbit polyclonal anti-ASF1A	Cell Signaling Technology	Cat#: 2990
Rabbit polyclonal anti-ASF1B	Cell Signaling Technology	Cat#: 2902
Rabbit polyclonal anti-TLK1	Cell Signaling Technology	Cat#: 4125
Rabbit polyclonal anti-TLK2	Bethyl Laboratories	Cat#: A301-257A
Rabbit polyclonal anti-phospho ASF1A (Ser166)	Groth Laboratory	(Klimovskaia et al., 2014)
Rabbit polyclonal anti-phospho p53 (Ser15)	Cell Signaling Technology	Cat#: 9284
Rabbit monoclonal anti-phospho H2AX (Ser139)	Cell Signaling Technology	Cat#: 9718
Rabbit polyclonal anti-phospho Chk2 (Thr68)	Cell Signaling Technology	Cat#: 2661
Rabbit polyclonal anti-phospho RPA32 (Ser4/Ser8)	Bethyl Laboratories	Cat#: A300-245A
Mouse anti-p53	Cell Signaling Technology	Cat#: 2524
Mouse anti-p21	BD Biosciences	Cat#:556430
Actin (clone C4)	EMD Millipore	Cat#: MAB1501
GAPDH (6C5)	Thermofisher	Cat#: AM4300
CD11b (APC, Rat)	eBioscience	Cat#: 50-112-9622
CD19 (1D3, APC-eFluor 780)	eBioscience	Cat#: 47-0193-82
CD3 (PE-Cy7, Hamster)	BD Biosciences	Cat#: 552774
CD45 (PE)	eBioscience	Cat#: 12-0451-82
Ter-119 (Pacific Blue)	Biolegend	Cat#: 116232
Viability Dye (FVS510)	BD Biosciences	Cat#: 564406
CD135 (PercP-eFluor710)	eBioscience	Cat#: 46-1351-82
CD34 (Alexa700)	eBioscience	Cat#: 56-0341-82
CD117 (APC-eFluor780)	eBioscience	Cat#: 47-1171-82
CD150 (PE-Cy7)	Biolegend	Cat#: 115914
Sca-1 (Pacific Blue)	Biolegend	Cat#: 108120
CD48 (BV711)	BD BioSciences	Cat#: 740687
CD3 (APC)	eBioscience	Cat#: 50-148-41
CD4 (APC)	eBioscience	Cat#: 50-148-54
CD8 (APC)	eBioscience	Cat#: 17-0081-82
B220/CD45R (APC)	eBioscience	Cat#: 17-0452-82
Gr-1 (APC)	BioLegend	Cat#: 108412
Ter-119 (APC)	eBioscience	Cat#: 17-5921-82
CD-19 (APC)	eBioscience	Cat#: 50-149-09
IgM (APC)	eBioscience	Cat#: 17-5790-82
CD127 (APC)	eBioscience	Cat#: 17-1271-82
Anti-human CD33 (PE-Cy7)	eBioscience	Cat#: 25-0338-42
Anti-human CD13 (PE-Cy7)	BD Bioscience	Cat#: 561599
Anti-human CD45 (BV650)	Biolegend	Cat#: 304044
Anti-human CD15 (V450)	BD Bioscience	Cat#: 642922
Anti-mouse CD45 (APC-Cy7)	BD Bioscience	Cat#: 557659

Fixable aqua dye	Thermo Fisher Scientifc	Cat#: L34957
Bacterial and Virus Strains		
Bacteria: TOP10 Chemically Competent E. coli	Thermo Fisher Scientific	Cat#:C404003
Lentivirus: shASF1A		
Lentivirus: shASF1B		
Lentivirus: shTLK1		
Lentivirus: shTLK2		
Lentivirus: shNT16		
Lentivirus: shNT17		
Biological Samples		
Primary AML cells	This study	Table S1
Healthy bone marrow	Lonza	
Chemicals, Peptides, and Recombinant Proteins		
Methocult M3234	STEMCELL Technologies	Cat#: 03234
Methocult H4230	STEMCELL Technologies	Cat#: 04234
Murine IL-1β	PeproTech	Cat#: 211-11B-100UG
Murine IL-3	PeproTech	Cat#: 213-13-2UG
Murine IL-6	PeproTech	Cat#: 216-16-2UG
Murine SCF	PeproTech	Cat#: 250-03-10UG
Puromycin	Gibco	Cat#: A1113803
Doxycycline chow	Envigo	Cat#: D11072801
Doxycycline hyclate	Sigma-Aldrich	Cat#: D9891
Doramapimod	Selleck	Cat#: S1574
Critical Commercial Assays		
Direct Lineage Cell Depletion Kit (Mouse)	Miltenyi Biotec	Cat#: 130-110-470
CD34 MicroBead Kit (Human)	Miltenyi Biotec	Cat#: 130-046-702
High-Capacity cDNA Reverse Transcription Kit	Thermo Fisher Scientific	Cat#: 4368814
RNeasy mini kit	Qiagen	Cat#: 217004
Gateway LR Clonase Enzyme Mix	Thermo Fisher Scientific	Cat#: 11791-100
Platinum SYBR Green qPCR SuperMix	Thermo Fisher Scientific	Cat#: 11733-046
Deposited Data		
Raw and processed data (RNA-Seq in bone marrow from healthy and primary AML cells)	This study	GSE
Experimental Models: Cell Lines		
MOLM-14	ATCC	
Experimental Models: Organisms/Strains		
C56BL/6J	Jackson Labs	000664

NOD.Cg-Prkdcscid Il2rgtm1Wjl Tg(CMV-IL3,CSF2,KITLG)1Eav/MloySzJ (NSGS)	Jackson Labs	013062
NSG		
B6.Cg-Commd10Tg(Vav1-icre)A2Kio/J (Vav-iCre)	Jackson Labs	008610
C57BL/6NJ-Asf1bem1(IMPC)J/Mmjax	Jackson Labs	042325
Vav-Cre TLK2	This study	
Recombinant DNA		
pMSCV-IRES-mCherry FP	Addgene	#52114
mCherry-ASF1B	This study	
EcoPac		
Software and Algorithms		
FlowJo		
Prism 9	Graphpad	https://www.graphpad.com/
Adobe Illustrator	Adobe	
Image Lab	BioRad	
RNA-Seq analysis		

SPRINGER NATURE LICENSE
TERMS AND CONDITIONS

Jun 20, 2022

This Agreement between Hsin-Yun Lin ("You") and Springer Nature ("Springer Nature") consists of your license details and the terms and conditions provided by Springer Nature and Copyright Clearance Center.

License Number	5333281039538
License date	Jun 20, 2022
Licensed Content Publisher	Springer Nature
Licensed Content Publication	Cellular and Molecular Life Sciences
Licensed Content Title	The Tousled-like kinases regulate genome and epigenome stability: implications in development and disease
Licensed Content Author	Sandra Segura-Bayona et al
Licensed Content Date	Jul 13, 2019
Type of Use	Thesis/Dissertation
Requestor type	academic/university or research institute
Format	electronic
Portion	figures/tables/illustrations
Number of figures/tables/illustrations	2
Will you be translating?	no
Circulation/distribution	30 - 99
Author of this Springer Nature content	no
Title	IDENTIFICATION OF TLK/ASF1 AS A NOVEL PATHWAY FOR MEDIATING IL-1b-DRIVEN ACUTE MYELOID LEUKEMIA
Institution name	Oregon Health & Science University
Expected presentation date	Sep 2022

Portions	I will be using human TLK structure schematic in Figure 1 and human ASF1 structure schematic in Figure 2.
	Hsin-Yun Lin 2720 SW Moody Ave 2nd Floor
Requestor Location	PORTLAND, OR 97201 United States Attn: Hsin-Yun Lin
Total	0.00 USD

Terms and Conditions

Springer Nature Customer Service Centre GmbH
Terms and Conditions

This agreement sets out the terms and conditions of the licence (the **Licence**) between you and **Springer Nature Customer Service Centre GmbH** (the **Licensor**). By clicking 'accept' and completing the transaction for the material (**Licensed Material**), you also confirm your acceptance of these terms and conditions.

1. Grant of License

1. 1. The Licensor grants you a personal, non-exclusive, non-transferable, world-wide licence to reproduce the Licensed Material for the purpose specified in your order only. Licences are granted for the specific use requested in the order and for no other use, subject to the conditions below.

1. 2. The Licensor warrants that it has, to the best of its knowledge, the rights to license reuse of the Licensed Material. However, you should ensure that the material you are requesting is original to the Licensor and does not carry the copyright of another entity (as credited in the published version).

1. 3. If the credit line on any part of the material you have requested indicates that it was reprinted or adapted with permission from another source, then you should also seek permission from that source to reuse the material.

2. Scope of Licence

2. 1. You may only use the Licensed Content in the manner and to the extent permitted by these Ts&Cs and any applicable laws.

2. 2. A separate licence may be required for any additional use of the Licensed Material, e.g. where a licence has been purchased for print only use, separate permission must be obtained for electronic re-use. Similarly, a licence is only valid in the language selected and does not apply for editions in other languages unless additional translation rights have been granted separately in the licence. Any content owned by third parties are expressly excluded from the licence.

2. 3. Similarly, rights for additional components such as custom editions and derivatives require additional permission and may be subject to an additional fee. Please apply to Journalpermissions@springernature.com/bookpermissions@springernature.com for these rights.

2. 4. Where permission has been granted **free of charge** for material in print, permission may also be granted for any electronic version of that work, provided that the material is incidental to your work as a whole and that the electronic version is essentially equivalent to, or substitutes for, the print version.

2. 5. An alternative scope of licence may apply to signatories of the STM Permissions Guidelines, as amended from time to time.

3. Duration of Licence

3. 1. A licence for is valid from the date of purchase ('Licence Date') at the end of the relevant period in the below table:

Scope of Licence	Duration of Licence

Post on a website	12 months
Presentations	12 months
Books and journals	Lifetime of the edition in the language purchased

4. Acknowledgement

4. 1. The Licensor's permission must be acknowledged next to the Licenced Material in print. In electronic form, this acknowledgement must be visible at the same time as the figures/tables/illustrations or abstract, and must be hyperlinked to the journal/book's homepage. Our required acknowledgement format is in the Appendix below.

5. Restrictions on use

5. 1. Use of the Licensed Material may be permitted for incidental promotional use and minor editing privileges e.g. minor adaptations of single figures, changes of format, colour and/or style where the adaptation is credited as set out in Appendix 1 below. Any other changes including but not limited to, cropping, adapting, omitting material that affect the meaning, intention or moral rights of the author are strictly prohibited.

5. 2. You must not use any Licensed Material as part of any design or trademark.

5. 3. Licensed Material may be used in Open Access Publications (OAP) before publication by Springer Nature, but any Licensed Material must be removed from OAP sites prior to final publication.

6. Ownership of Rights

6. 1. Licensed Material remains the property of either Licensor or the relevant third party and any rights not explicitly granted herein are expressly reserved.

7. Warranty

IN NO EVENT SHALL LICENSOR BE LIABLE TO YOU OR ANY OTHER PARTY OR ANY OTHER PERSON OR FOR ANY SPECIAL, CONSEQUENTIAL, INCIDENTAL OR INDIRECT DAMAGES, HOWEVER CAUSED, ARISING OUT OF OR IN CONNECTION WITH THE DOWNLOADING, VIEWING OR USE OF THE MATERIALS REGARDLESS OF THE FORM OF ACTION, WHETHER FOR BREACH OF CONTRACT, BREACH OF WARRANTY, TORT, NEGLIGENCE, INFRINGEMENT OR OTHERWISE (INCLUDING, WITHOUT LIMITATION, DAMAGES BASED ON LOSS OF PROFITS, DATA, FILES, USE, BUSINESS OPPORTUNITY OR CLAIMS OF THIRD PARTIES), AND
WHETHER OR NOT THE PARTY HAS BEEN ADVISED OF THE POSSIBILITY OF SUCH DAMAGES. THIS LIMITATION SHALL APPLY NOTWITHSTANDING ANY FAILURE OF ESSENTIAL PURPOSE OF ANY LIMITED REMEDY PROVIDED HEREIN.

8. Limitations

8. 1. ***BOOKS ONLY:***Where **'reuse in a dissertation/thesis'** has been selected the following terms apply: Print rights of the final author's accepted manuscript (for clarity, NOT the published version) for up to 100 copies, electronic rights for use only on a personal website or institutional repository as defined by the Sherpa guideline (www.sherpa.ac.uk/romeo/).

8. 2. For content reuse requests that qualify for permission under the STM Permissions Guidelines, which may be updated from time to time, the STM Permissions Guidelines supersede the terms and conditions contained in this licence.

9. Termination and Cancellation

9. 1. Licences will expire after the period shown in Clause 3 (above).

9. 2. Licensee reserves the right to terminate the Licence in the event that payment is not received in full or if there has been a breach of this agreement by you.

Appendix 1 — Acknowledgements:

For Journal Content:
Reprinted by permission from [**the Licensor**]: [**Journal Publisher** (e.g. Nature/Springer/Palgrave)] [**JOURNAL NAME**] [**REFERENCE CITATION** (Article name, Author(s) Name), [**COPYRIGHT**] (year of publication)

For **Advance Online Publication papers:**
Reprinted by permission from [**the Licensor**]: [**Journal Publisher** (e.g. Nature/Springer/Palgrave)] [**JOURNAL NAME**] [**REFERENCE CITATION** (Article name, Author(s) Name), [**COPYRIGHT**] (year of publication), advance online publication, day month year (doi: 10.1038/sj.[JOURNAL ACRONYM].)

For Adaptations/Translations:
Adapted/Translated by permission from [**the Licensor**]: [**Journal Publisher** (e.g. Nature/Springer/Palgrave)] [**JOURNAL NAME**] [**REFERENCE CITATION** (Article name, Author(s) Name), [**COPYRIGHT**] (year of publication)

Note: For any republication from the British Journal of Cancer, the following credit line style applies:

Reprinted/adapted/translated by permission from [**the Licensor**]: on behalf of Cancer Research UK: : [**Journal Publisher** (e.g. Nature/Springer/Palgrave)] [**JOURNAL NAME**] [**REFERENCE CITATION** (Article name, Author(s) Name), [**COPYRIGHT**] (year of publication)

For **Advance Online Publication** papers:
Reprinted by permission from The [**the Licensor**]: on behalf of Cancer Research UK: [**Journal Publisher** (e.g. Nature/Springer/Palgrave)] [**JOURNAL NAME**] [**REFERENCE CITATION** (Article name, Author(s) Name), [**COPYRIGHT**] (year of publication), advance online publication, day month year (doi: 10.1038/sj.[JOURNAL ACRONYM])

For Book content:
Reprinted/adapted by permission from [**the Licensor**]: [**Book Publisher** (e.g. Palgrave Macmillan, Springer etc) [**Book Title**] by [**Book author**(s)] [**COPYRIGHT**] (year of publication)

Other Conditions:

Version 1.3

Questions? customercare@copyright.com or +1-855-239-3415 (toll free in the US) or +1-978-646-2777.